

Seismic stratigraphy and depositional architecture of Neogene intraslope basins, offshore western Niger Delta

Kelvin Chima, Damien Do Couto, Estelle Leroux, Silvia Gardin, Nick Hoggmascall, Marina Rabineau, Didier Granjeon, Christian Gorini

▶ **To cite this version:**

Kelvin Chima, Damien Do Couto, Estelle Leroux, Silvia Gardin, Nick Hoggmascall, et al.. Seismic stratigraphy and depositional architecture of Neogene intraslope basins, offshore western Niger Delta. Marine and Petroleum Geology, 2019, 109, pp.449-468. 10.1016/j.marpetgeo.2019.06.030 . hal-02329251

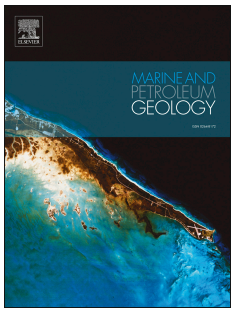
HAL Id: hal-02329251
https://hal.science/hal-02329251

Submitted on 30 Oct 2019

HAL is a multi-disciplinary open access archive for the deposit and dissemination of scientific research documents, whether they are published or not. The documents may come from teaching and research institutions in France or abroad, or from public or private research centers.

L'archive ouverte pluridisciplinaire **HAL**, est destinée au dépôt et à la diffusion de documents scientifiques de niveau recherche, publiés ou non, émanant des établissements d'enseignement et de recherche français ou étrangers, des laboratoires publics ou privés.

Accepted Manuscript



Seismic stratigraphy and depositional architecture of Neogene intraslope basins, offshore western Niger Delta

Kelvin I. Chima, Damien Do Couto, Estelle Leroux, Silvia Gardin, Nick Hoggmascall, Marina Rabineau, Didier Granjeon, Christian Gorini

PII: S0264-8172(19)30282-X

DOI: https://doi.org/10.1016/j.marpetgeo.2019.06.030

Reference: JMPG 3891

To appear in: *Marine and Petroleum Geology*

Received Date: 23 November 2018

Revised Date: 14 June 2019

Accepted Date: 16 June 2019

Please cite this article as: Chima, K.I., Do Couto, D., Leroux, E., Gardin, S., Hoggmascall, N., Rabineau, M., Granjeon, D., Gorini, C., Seismic stratigraphy and depositional architecture of Neogene intraslope basins, offshore western Niger Delta, *Marine and Petroleum Geology* (2019), doi: https://doi.org/10.1016/j.marpetgeo.2019.06.030.

This is a PDF file of an unedited manuscript that has been accepted for publication. As a service to our customers we are providing this early version of the manuscript. The manuscript will undergo copyediting, typesetting, and review of the resulting proof before it is published in its final form. Please note that during the production process errors may be discovered which could affect the content, and all legal disclaimers that apply to the journal pertain.

ACCEPTED MANUSCRIPT

Seismic stratigraphy and depositional architecture of Neogene intraslope basins, offshore western Niger Delta

Kelvin I. Chima[a,b]*, Damien Do Couto[a], Estelle Leroux[c], Silvia Gardin[d], Nick Hoggmascall[e], Marina Rabineau[f], Didier Granjeon[g], Christian Gorini[a]

[a] Sorbonne Université-ISTeP UMR 7193, Paris (France)

[b] Alex Ekwueme Federal University, Ndufu-Alike Ikwo, Ebonyi State, Nigeria.

[c] IFREMER, ZI Pointe du Diable, Plouzane, France (France)

[d] Centre de Recherche en paléontologie Paris, UMR 7207

[e] Shell Petroleum Development Company, Lagos (Nigeria).

[f] CNRS, UMR 6538, LGO (CNRS/UBO/UBS), Plouzane (France)

[g] IFPEN, Rueil-Malmaison (France)

Abstract

Located on a divergent margin dominated by gravity tectonics above overpressured marine shales, the Niger Delta slope has been described as having a stepped profile characterized by 'filled ponded basins' that are prone to erosion and sediment bypass. Previous studies based on 3D seismic data have described the depositional architecture of the western Niger Delta's upper slope, but calibration of the seismic facies is lacking and the timing of major changes in sedimentary record remains elusive. In this study, seismic sequence-stratigraphy, 3D geomorphological analyses of high-resolution 3D seismic data, and bio/chronostratigraphic analyses from four boreholes, enabled the identification and characterization of the depositional architecture in Neogene 'filled ponded basins'. Seven major seismic units were dated as

Chattian, Burdigalian, Serravallian, Tortonian, Middle Pliocene and Middle Pleistocene to the present day. Major changes in the sedimentary record occurred in the Plio-Pleistocene, with the onset of erosive channel levee systems (CLSs) and mass-transport deposits (MTDs) generally capped by a hemipelagic drape. Amalgamated CLSs characterize the Tortonian-Late Miocene while erosive MTDs and CLSs characterize the Plio-Pleistocene units. Thick, laterally extensive MTDs are associated with regional slope instability, while active mobile shale triggered local spatially confined MTDs. Submarine channels evolved from moderate to highly sinuous. The degree of channel confinement generally decreases downstream where they are characterized by abandoned meander loops and avulsion resulting from levee breaching. Channel fills and levees/overbank deposits topped by hemipelagic drapes provide effective reservoir/seal (traps) for hydrocarbons. The alternation of channel deposits and hemipelagic layers indicate that eustasy controlled depositional patterns at a regional scale, while the spatio-temporal switches in submarine channel courses show that shale tectonics locally controlled deposition in intraslope basins.

Keywords: West Africa; Niger Delta; Seismic sequence stratigraphy; Filled ponded basins; Mass-transport deposits; Turbidite systems; Chronostratigraphy.[1]

1. Introduction

[a,b*] Corresponding author : Kelvin Ikenna Chima; Sorbonne University; *Institut des Sciences de la Terre* (*ISTeP*), Case 129, Tour 56/66, fifth floor, 4 Place Jussieu, 75252, Paris Cedex. E-mail: kelvini.chima@gmail.com

The depositional architecture of the deep-water systems located on divergent margins is predominantly controlled by gravity tectonics (e.g. Doust and Omatsola, 1990; Damuth, 1994; Cohen and McClay, 1996; Morely and Guerin, 1996; Graue, 2000; Cobbold *et al.*, 2009). Gravity gliding and gravity spreading are the two main aspects of gravity tectonics that deform the sedimentary wedges that prograde into deep-water environments (Morley *et al.*, 2011). While gravity gliding is characterized by the rigid translation of a rock mass down a slope, gravity spreading results from flattening and lateral spreading of a rock mass under its own weight (Ramberg, 1981; Dejong and Sholten, 1973; Alves and Lourenço, 2010; Alves, 2015). In the Niger Delta, gravity spreading driven by delta wedge progradation above overpressured marine shales has been described as the primary control of accommodation and depositional patterns (e.g. Doust and Omatsola, 1990; Damuth, 1994; Cohen and McClay, 1996; Morely and Guerin, 1996; Graue, 2000; Cobbold *et al.*, 2009).

The slope of the Niger Delta, characterized by a lower subsidence rate than its regional sedimentation rate, has been described as comprising a 'stepped profile', compared to the 'above-grade slope profile' typical of the central Gulf of Mexico-where the rate of salt driven subsidence is always greater than that of sediment supply (Prather, 2003). Consequently, 'shallow ponded basins/perched accommodation' described by Prather *et al.* (2012a), but herein referred to as 'filled ponded basins', dominate the intra-slope regions of the Niger Delta (Booth *et al.*, 2000; Prather, 2000). These 'filled ponded basins' are dominated by healed-slope accommodation that is always overfilled or bypassed compared to the underfilled ponded basins in the central Gulf of Mexico (Prather, 2003). Although the lack of ponded accommodation in the upper-and mid-slope regions of the Niger Delta renders it susceptible to erosion and bypass, thin reservoir facies associated with channel and overbank deposits in these areas could still be

good drilling targets (Prather, 2003). Furthermore, hydrocarbon traps are better developed in filled ponded systems, where reservoir facies occur directly below mud-rich pelagic/hemipelagic deposits (Prather, 2003).

Following the discovery of hydrocarbons in the deep-water Niger Delta in recent decades, exploration is now focused on understanding the control on depositional architecture and reservoir distribution in the deep-water setting of this region (e.g. Chapin *et al.*, 2002; Adeogba *et al.*, 2005). Consequently, the impact on submarine channel evolution and depositional patterns by mobile shale structures has received considerable attention (e.g. Adeogba *et al.*, 2005; Olusola *et al.*, 2007; Clark and Cartwright, 2012; Prather *et al.*, 2012a, Jobe *et al.*, 2015; Jolly *et al.*, 2016; Hansen *et al.*, 2017). The depositional architecture of the Pliocene and Quaternary filled ponded basins on the western slope of the Niger Delta has already been described and includes MTDs and turbidite systems draped by hemipelagites (e.g. Adeogba *et al.*, 2005; Olusola *et al.*, 2007). Similar depositional architectures have been described in the deep-water fold-and-thrust belt of the Niger Delta (e.g. Posamentier and Kolla, 2003; Clark and Cartwright, 2012). Recently, academic seismic-stratigraphic studies were conducted on the deeper Neogene stratigraphic records of the upper slope of the western Niger Delta, although lacking calibration (Benjamin *et al.*, 2015; Benjamin and Huuse, 2017). Industry-based study of Neogene stratigraphy reveals that highly amalgamated channel fill deposits are less compartmentalized than less amalgamated overbank deposits (Chapin *et al.*, 2002).

Despite the plethora of observations on the upper slope of the western Niger Delta, lack of published borehole and bio/chronostratigraphic data has limited seismic facies calibration and age estimates for the entire Neogene succession in this region. Similarly, no study has investigated the interactions between shale tectonics and submarine channels/reservoir

distribution in the study area (Fig. 1). Hence, the objectives of this study are to: (1) identify and date major sequence-stratigraphic surfaces (Neogene to present day) preserved on the upper slope of the western Niger Delta; (2) calibrate seismic facies by defining depositional environments to better the understanding of depositional patterns and their controlling factors; (3) investigate the interaction between shale tectonics and depositional patterns with a view to predicting reservoir distribution in the associated 'filled ponded basins'. This study not only provides age constraints on the Neogene stratigraphy of the western Niger Delta, but also describes the effect of the interplay between autogenic and allogenic forcing on the depositional architecture and potential reservoir distribution in 'filled ponded basins'.

2. Geological setting

The Niger Delta is located along the Equatorial Atlantic margin of West Africa (Fig. 1). The delta is underlain by sub-aerial and submarine sediments covering an area of ~140,000 km^2; and its thickness reaches 12 km (Allen, 1965; Evamy *et al.*, 1978; Doust and Omatsola, 1990). The progradation of this siliciclastic wedge since the Late Eocene has been estimated as ~300 km (Doust and Omatsola, 1990; Fig. 1). Known oil and gas resources rank the delta the twelfth largest petroleum province in the world (Tuttle *et al.*, 1999). The Niger Delta is sub-divided into three major structural domains: (i) an extensional zone below the continental shelf, (ii) a transitional zone below the upper slope, and (iii) a compressional zone located at the toe of the slope (Doust and Omatsola, 1990; Damuth, 1994; Connors *et al.*, 1998; Morgan, 2004; Billoti and Shaw, 2005; Fig. 1).

The stratigraphy of the Niger Delta is dominated by three major lithostratigraphic units: the Akata, Agbada and Benin Formations (Short and Stauble, 1967; Evamy *et al*., 1978; Avbovbo, 1978; Doust and Omatsola, 1990; Fig. 2). The Akata Formation comprises marine shales that range in thickness from 7,000 m beneath the continental shelf to 2,000 m in the distal portion (Doust and Omatsola, 1990). Its thickness reaches 5,000 m in the deep fold-and-thrust belt due to the repeated occurrence of thrust ramps (Wu and Bally, 2000; Corredor *et al*., 2005). The Agbada Formation constitutes the deltaic unit of the Niger Delta. The thickness of this paralic unit reaches 3,500 m (Evamy *et al*., 1978; Avbovbo *et al*., 1978; Doust and Omatsola, 1990). The depositional setting of this lithostratigraphic unit ranges from delta-front, delta-topset to fluvio-deltaic environments (Avbovbo, 1978). The Benin Formation consists of alluvial to upper coastal plain deposits up to 2,000 m thick (Avbovbo, 1978). The Agbada and Benin Formations are associated with clay-filled channels that were incised during the Late Miocene and Plio-Quaternary (Fig. 2).

The present study is focused on the mobile shale belt located on the upper continental slope downward the transition between the extensional and compressional belts, offshore western Niger Delta (Fig. 1; red square). It covers 638 km^2 at a distance of ~120 km from the present day coastline (Fig. 1), at depths ranging from 900 to 1,150 m within the Akata Formation, which is located at water depths between ~810 to ~3240 m. The area is characterized by 'filled ponded basins' located at the flanks of mobile shales and ~3 km wide NE-SW trending submarine channel complex extending more than 25 km into the 3D block studied (Fig. 3). The reservoir compartmentalization of the block has already been investigated by Chapin *et al* (2002) and seabed mounds and pockmarks by Benjamin *et al*. (2015); Benjamin and Huuse (2017).

3. Dataset and methods

3.1 Dataset

The dataset used in this study includes high-resolution 3D seismic and borehole data, comprising well logs, core and biostratigraphic data.

3.1.1 Seismic data

The 3D seismic data were processed as a zero-phase source wavelet in American reverse standard polarity. Thus, an increase in acoustic impedance corresponds to a trough (blue loop) in the wavelet, while a decrease in acoustic impedance is represented by a peak (red loop) in the wavelet. The horizontal resolution of the data is characterized by a stacking bin spacing of 25 m x 25 m (in-line and cross-line spacing), and a seismic recording sampling interval of 4 milliseconds two-way travel time (TWT). The dominant frequency of the data is 30 Hz over the first 3 seconds (TWT) but decreases between 20-25 Hz below a depth of 3 km. Using average interval seismic velocity of 1,639.4 m/s and applying the velocity-wavelength equation ($\lambda/4$; Brown, 1999), the vertical resolution of the data was ~13.7 m over the Pliocene-Quaternary intervals but decreased between 25 and 30 m at depths below 3 km.

3.1.2 Borehole data

154 The lithology, facies and depositional environments of five boreholes, labelled FM-1,
155 FM-2, FM-3ST1, FM-4ST1 and FM-5 located in the southern part of the study area (Fig. 3),
156 were analyzed. The wells penetrated respective total depths of 4,154 m, 3,627 m, 2,924 m, 3,458
157 m and 3,497 m below the seafloor. Petrophysical (gamma-ray, resistivity, neutron, density and
158 sonic) logs were acquired mostly in the deeper stratigraphic intervals, e.g. between 1,140-4,154
159 m in the deepest FM-1 well and 1,718-2,119 m in the shallowest FM-3ST1 well. Four of the five
160 boreholes contain biostratigraphic data, whereas core data were only available in two boreholes.
161
162 3.2 Methods
163
164 3.2.1 Seismic and sequence stratigraphic analysis
165
166 A standard seismic-stratigraphic analysis approach (Mitchum *et al.,* 1977) was used for
167 the 3D seismic data based on the recognition of reflection termination patterns such as onlap,
168 erosional truncations, seismic facies/configuration and vertical stacking patterns. Previously
169 described depositional architectures include MTDs, turbidite systems and hemipelagic drapes. In
170 the present study, MTDs and turbidite deposits were identified based on seismic criteria and 3D
171 geomorphology (e.g. Posamentier and Kolla, 2003; Richardson, 2011). MTDs were recognized
172 (i) by their basal shear zone or basal continuous surface, which delimits the overlying deformed
173 materials and the underlying, relatively continuous materials (Frey Martinez *et al.*, 2005; Alves
174 and Lourenço, 2010; Gamberi *et al.*, 2011; 2015) and (ii) by their top, characterized by
175 rugose/irregular topographies (Richardson, 2011). In terms of internal architecture, MTDs may
176 be chaotic or transparent depending on (i) the nature of materials inherited from the source area

(Masson *et al.,* 2006), and (ii) the distance from source area (e.g. Alves *et al.,* 2009; Omosanya and Alves, 2013; Rovere *et al.,* 2014; Omosanya and Harishidayat, 2019). Turbidite systems were recognized based on the presence of sandy submarine channel deposits, which are generally characterized by high to moderate seismic reflectivity and high root mean square (RMS) amplitudes on 3D paleo-geomorphological maps (see also Posamentier and Kolla, 2003; Catuneanu, 2006). Drapes were interpreted as the result of a combination of pelagic/hemipelagic suspension fall-out as well as from the fine-grained suspended portion of turbidity flows (Kneller and McCaffrey, 1999).

3.2.2 Well logs, lithofacies and depositional environment

The standard approach to well-log analysis (e.g. Mitchum *et al.,* 1977) is the display and visual inspection of accurately scaled gamma-ray, neutron-density cross plots, resistivity and sonic logs. Integrated analysis of these logs and calibration with core data helped delineate lithofacies and associated depositional environments.

3.2.3 Bio- and chronostratigraphic analyses

We analyzed existing biostratigraphic data, chiefly calcareous nannofossils and planktonic foraminifera, from ditch cutting samples available in four boreholes. This allowed us to constrain the ages of Neogene stratigraphic intervals.

3.2.4 3D Seismic geomorphology

In addition to 2D seismic stratigraphy, we conducted 3D seismic geomorphological analyses to identify erosional features and channel architectures, and to distinguish main depositional elements (mass-flow deposits, channel deposits, overbank deposits, mud volcanoes and hemipelagic units). This was achieved through a detailed analysis of seismic attributes, horizon slices and amplitude maps (after Posamentier and Kolla, 2003; Catuneanu, 2006).

Seismic attributes are all observations extracted from seismic data that directly or indirectly facilitate hydrocarbon identification, lithological discrimination or geological interpretation (Chopra and Marfurt; 2007; Taner *et al.*, 1994). We generated RMS and Variance Edge/Coherence attributes from the original 3D seismic data using Petrel™ software. The RMS attribute computes the square root of the sum of squared amplitudes over the geological interval of interest and facilitates lithofacies discrimination (e.g. Catuneanu, 2006). The variance attribute (e.g. Fig. 3D) emphasizes the correlation of seismic traces by assigning light colors to areas where seismic traces correlate (low variance) and dark colors to areas where there is no correlation (high variance; Fig. 3D; see Catuneanu, 2006). This attribute was used to delineate structural and stratigraphic discontinuities such as faults, mobile shales, turbidite systems, MTDs etc.

4. Results and interpretation

This section presents the results of seismic facies analysis and lithofacies description, depositional environments and depositional architectures within the stratigraphic intervals we

studied. Seismic artefacts (sensu Chopra and Marfurt, 2007; Alves, 2015) in the studied 3D volume is characterized by seismic wipe out in mobile shales zones (e.g. Fig. 5).

4.1. Seismic facies analysis and seismic stratigraphic units

4.1.1 Seismic facies analysis

Six seismic facies were identified in the studied 3D volume (Fig. 4) using the seismic facies classification schemes proposed by Prather *et al.* (1998) and Hanson *et al.* (2017). These include: (1) chaotic, discontinuous low amplitude seismic facies (B_l), generally characterized by an erosive base, irregular top and deformed internal architecture interpreted as mass-transport deposits (MTDs); (2) chaotic, discontinuous, high amplitude seismic facies (B_h) interpreted as turbidite feeder channels; (3) inclined, coherent/moderately deformed, high amplitude seismic facies interpreted as slides/slump blocks; (4) parallel, continuous/convergent, high amplitude seismic facies (C_{bh}) interpreted as amalgamated channels/lobes; (5) convergent thinning high amplitude seismic facies (C_{th}) flanked by seismic packages that onlap negative topographic relief features interpreted as levees and channel fill deposits, respectively; (6) transparent, continuous seismic facies (D) interpreted as hemipelagic drapes.

4.1.2 Seismic stratigraphic units

Seven major seismic stratigraphic units were identified in the Neogene stratigraphic records of the upper slope of the western Niger Delta (Fig. 5).

245

246 Unit 1

247 This is the oldest stratigraphic unit identified in the study area. This unit has not been
248 drilled. It is characterized by high amplitude seismic packages whose base corresponds to the top
249 of the reflection-free (low reflectivity) seismic unit (Fig. 5). Seismic reflectivity in Unit 1
250 generally decreases toward the north corresponding to a vertical, irregular, seismic wipeout zone
251 that extends upwards from 6 to 1.8 seconds (twt) deforming the overlying seabed (Fig. 5). This
252 feature was interpreted as mobile shale. Unit 1 thins from north and south toward the mobile
253 shale zone in the north (Fig. 5). The overall thinning of seismic Unit 1 from the south to the
254 north toward mobile shale indicates syn-kinematic deformation linked to the movement of
255 mobile shale during the deposition of Unit 1 (Fig. 5).

256

257 Unit 2

258 The base of Unit 2 shows baselap (apparent onlap) surface overlain by parallel to sub-
259 parallel, moderate to high amplitude seismic packages that generally decrease in reflectivity
260 northward due to the presence of mobile shale (Fig. 5). Seismic packages within this unit are
261 generally subparallel and thin northward except within a landward dipping normal fault near the
262 mobile shale zone (Fig. 5).

263

264 Unit 3.

265 The base of unit 3 is also a baselap (apparent onlap) surface overlain by parallel
266 continuous, high amplitude seismic packages whose reflectivity decreases northward toward the
267 mobile shale zone (Fig. 5). Although Unit 3 reaches maximum thickness within a fault-

268 controlled accommodation in the southern part, it thins northward toward the mobile shale zone
269 (Fig. 5).
270
271 Unit 4
272 The base of unit 4 is locally erosional and marks a transition from underlying parallel,
273 continuous high amplitude seismic packages to overlying moderate to high amplitude strata (Fig.
274 5). Unit 4 is characterized by localized high amplitude seismic packages that generally converge
275 or thin away from their central parts toward their lateral limits (Fig. 5). These seismic packages
276 are interpreted as amalgamated channel levee deposits (dotted purple circles in Fig. 5). Although
277 Unit 4 also reaches maximum thickness in fault-controlled accommodation in the southern part,
278 it thins northward toward the mobile shale zone (Fig. 5).
279
280 Unit 5
281 Unit 5 is marked at the base by an erosional event overlain by thin, discontinuous/chaotic,
282 low amplitude seismic packages that grade to relatively continuous, high amplitude seismic
283 packages near the mobile shale zone (Fig. 5). Seismic geometries in Unit 5 vary from sub-
284 parallel (north and south) in the mobile shale zone to convergent/thinning toward the mobile
285 shale zone (Fig. 5). Unit 5 is characterized by amalgamated, high amplitude seismic packages
286 corresponding to the channel levee deposits described above (dotted purple circles in Fig. 5). An
287 over 80 m-thick transparent seismic unit interpreted as an hemipelagic drape overlies this unit
288 (Fig. 5). This hemipelagic layer was truncated by younger channel levee systems (CLSs) that
289 locally incised the underlying deposits by up to 40 m (Fig. 5). The thickness of Unit 5 remains
290 uniform in the south but thins northward toward the mobile shale zone.

291

292 Unit 6

293 The base of Unit 6 is erosional and marks a major change with the onset of erosive MTDs
294 and CLSs (Fig. 5). This erosional event can be traced throughout the studied 3D block except in
295 the northeast, where it could not be interpreted due to the combined effect of signal wipe out
296 (artefacts) and erosion (Fig. 5)**.** Three erosive mass-transport deposits labelled lower, middle and
297 upper MTDs were identified in unit 6 (Figs. 5, 6).

298 The lower MTD covers an area of ~155 km^2 and extends 3-5 km laterally with a
299 maximum thickness of ~148 m (using an average interval velocity of 1,639.4 m/s). Its upper
300 limit is relatively gentle with localized erosional scours (Fig. 5). This MTD truncates the
301 underlying CLS, reaching its maximum thickness at the northern and southern flanks, but drapes
302 the central area, where the CLS thins out (e.g. Figs. 5, 6 C, D, G).

303 The middle MTD covers an area of ~175 km^2 with a lateral distance of 6-8 km and
304 reaches maximum thickness of ~246 m in the hanging-wall block bounded by normal faults
305 labelled P, Q (see also Doust and Omatsola, 1990; Cohen McClay, 1996; Graue, 2000; Figs. 5,
306 6B, F). The middle MTD is followed by relatively continuous/chaotic, high amplitude seismic
307 packages interpreted as turbidite feeder channels. Unlike the lower MTD, the middle MTD is
308 highly deformed by synthetic and antithetic normal faults with inferred offsets of a few meters,
309 and 20-25 m relief incised into the underlying CLS (Figs. 5, 6F).

310 The upper MTD is the third and most laterally extensive MTD in Unit 6 (Fig. 5). It
311 covers an area of 187 km^2 with a lateral distance of 12 km and reaches a maximum thickness of
312 ~205 m downstream (Fig. 6A, E). This MTD also incises the underlying CLS, but was truncated
313 by younger turbidite feeder channels and affected by extensional deformation (Figs. 5, 6A, E).

The upper MTD is overlain by CLSs, ultimately draped by a hemipelagic layer that was truncated by younger CLSs (Fig. 5).

Unit 7

Unit 7 is the youngest seismic unit identified in the study area. Its base marks another major change in the sedimentary record, characterized by overall high-frequency and high-amplitude seismic packages (Fig. 5). These seismic packages are interpreted as amalgamated channel levee/lobe deposits and alternate with transparent seismic packages corresponding to hemipelagites (Fig. 5). The amalgamated channel levee/lobe deposits are locally truncated by turbidite feeder channels (Fig. 5). Unit 7 is topped by the seafloor, which is directly underlain by a thick hemipelagic deposit (Fig. 5).

4.2 Lithofacies and depositional environment

The integrated analysis of well logs in the study area shows that the intervals characterized by average to moderately high gamma-ray log values, low resistivity, high neutron-density separation and high sonic values correspond to hemipelagic layers, overbanks and/or mud-rich turbidites (e.g. Fig. 7). However, intervals defined by low gamma-ray, high resistivity, low neutron-density separation and low sonic values are interpreted as amalgamated channel deposits (Fig. 7). Facies vary from amalgamated channel sands at the base of submarine channel deposits to overbank and/or hemipelagic drape at the top (Fig. 7).

4.3 Bio/chronostratigraphic analyses and correlation with seismic data

Despite the location of the study area on the upper slope, which is prone to mass-wasting and sediment reworking, the integration of calcareous nannofossil and planktonic foraminifera biohorizons increased the reliability of the age model presented in this study.

We fixed the first occurrences (FOs), last occurrences (LOs), and the corresponding depths of key Neogene planktonic foraminifera (pf) and calcareous nannofossils (cn), in the biostratigraphic distribution sheet of the FM-1, FM-2, FM-3ST1 and FM-4 boreholes. We assigned ages to these fossil markers using equivalent ages derived from recently published studies (Anthonissen and Ogg, 2012; Backman *et al.*, 2012; Agnini *et al.*, 2014; Raffi *et al.*, 2016). Accordingly, the FO of *Sphenolithus ciperoensis* (cn) was assigned to ~24.4 Ma; the LO of *Cyclicargolithus abisectus* (cn) to ~23.5 Ma; the FO of *Globoquadrina dehiscens* (pf) to ~22.4 Ma; the FO and LO of *Sphenolithus heteromorphus* (cn) to ~17.5 Ma and ~13.53 Ma respectively; the LO of *Neogloboquadrina acostaensis* (pf) to ~9.8 Ma; the LO of *Cartinaster coalitus* (cn) to ~9.7 Ma (Fig. 7).

With the aid of time-depth relationship (checkshot) data, we depth-matched this bio/chronostratigraphic information with their corresponding seismic horizons. Finally, we attributed relative ages to the identified seismic reflectors based on: (i) the presence of fossil markers in at least two wells, with the exception of the LOs of *S. ciperoensis* (24.4 Ma) and *C. abisectus* (23.5 Ma), which were only recorded in the deepest FM-1 borehole. (ii) Relative depths of the identified seismic reflectors with respect to the nearest biohorizons (Figs. 5, 7, 8).

The basal limit of Unit 1 has not been drilled and could not be assigned a precise age (Figs. 5, 8). It tops the transparent seismic unit previously interpreted as deep-marine shales deposited during Eocene sea-level highstand e.g. Doust and Omatsols (1990). Also, it marks a

transition from the transparent seismic unit to the high amplitude seismic packages interpreted as turbidite deposits (amalgamated channels/lobes; e.g. Figs. 9, 13). The base of Unit 1 could be associated with an increase in sediment supply to the Niger Delta following the regional uplift that affected the area in the Oligocene (~34-28 Ma; Chardon *et al.*, 2016; Grimaud *et al.*, 2017).

The baselap (apparent onlap) associated with the base of Unit 2 (purple line in Fig. 5) occurs 200 m below the FO of *Sphenolithus ciperoensis* (~24.4 Ma), which occurs at the depth of 4,017.3 m in the FM-1 borehole (Fig. 7). The base of Unit 2 also could not be assigned a precise age since it has not been drilled (Fig. 7). The geometries of successive apparent onlaps (Fig. 5) suggests it is associated with a non-deposition period in the deep basin probably during maximum flooding of the shelf. Also, since it lies 200 m below the 24.4 Ma biohorizon, it could be a good candidate for the sea-level transgression described in the Chattian (Haq *et al.*, 1987; Fig. 8).

The base of Unit 3 (pink in Fig. 5) occurs 195 m above the LO of *Cyclicargolithus abisectus* (~23.5 Ma) and the FO of *Globoquadrina dehiscens* (~22.4 Ma; Figs. 5, 7). The base of this unit, defined by apparent onlaps, could also be a good candidate for a sea-level transgression in the Burdigalian (Haq *et al.*, 1987; Fig. 8). The older fossil marker-the LO of *C. abisectus* (~23.5 Ma), which was only recorded in the FM-1 borehole, occurs at the same depth as the younger fossil marker-the FO of *G. dehiscens* (~22.4 Ma), recorded in both FM-1 and FM-2 boreholes. These fossil markers are separated by ~1.1 Ma and should not coexist. Hence, this datum may represent a condensed interval or alternatively, *C. abisectus* could represent a reworked component. Since, the base of seismic Unit 3 lies 195 m above the FO of *G. dehiscens* ~22.4 Ma-Aquitanian (Figs. 7, 8), it could be related to the long-term Burdigalian sea-level transgression. It was tentatively assigned to the ~18.5 Ma (see Haq *et al.*, 1987; Fig. 8).

The base of seismic Unit 4 occurs 160 m above the LO of *Sphenolithus heteromorphus* (~13.53 Ma) and corresponds to a regional erosional truncation. This limit could be linked to the short-term sea-level fall in the Serravallian (~13.8 Ma) according to the Haq *et al.* (1987; Fig. 8), but probably occurred a little later in the Niger Delta. Since it is younger than 13.53 Ma, it was tentatively assigned to the Serravallian (~12.5 Ma).

The base of Unit 5 corresponds to a regional truncation and occurs 120 m above the LO of *Catinaster coalithus* (~9.7 Ma). Since this erosional event is younger than 9.7 Ma, it was assigned a tentative age of ~9.5 Ma on the assumption that it could be associated with the major progradation event recorded in the eastern Niger Delta during the Tortonian ~9.5 Ma (Jolly *et al.*, 2016).

On top of seismic Unit 5, we identified a transparent unit characterized in the FM-3ST1 borehole by abundant and diverse nannofossils and foraminifera. The LO of *Discoaster quinqueramus* (~5.5 Ma) allowed us to confidently date this hemipelagic layer as uppermost Messinian. At the top of this hemipelagic layer lies a barren interval, which is followed by an interval characterized by the simultaneous occurrence of *Reticulofenestra pseudoumbilicus* (cn), *Globorotalia plesiotumida* (pf), *Globorotalia miocenica* (pf), *Discoaster pentaradiatus* (cn), *Globorotalia exilis* (pf), *Discoaster brouweri* (cn) and *Gephyrocapsa spp* (cn). The co-occurrence of *D. brouweri* and *D. pentaradiatus*, whose extinction levels should be distinct in the uppermost Pliocene (Backman *et al*., 2012), together with the Pleistocene markers such as *H. sellii* and *Gephyrocapsa spp*, suggests that the top of this interval has been affected by reworking. The presence of a regional erosional event corresponds to this interval on seismic sections (e.g. red line in Figs. 5, 9B, 10C, 11C). It is characterized by the onset of erosive CLSs and MTDs.

Although we were unable to precisely define the Messinian-Pliocene transition due to poor biostratigraphic data, the onset of sediment-gravity flows following the hemipelagic drape dated ~5.5 Ma could be associated with sea-level fall following the transgressive event of the uppermost Messinian (Haq et *al.*, 1987). Therefore, the base of Unit 6 could be related to a sea-level fall in the Middle Pliocene (~3.7 Ma; see Haq *et al.*, 1987 curve recalibrated by Gorini *et al*; 2014; Fig. 8). This interpretation seems to agree with the progradation event recorded in the eastern Niger Delta during the Middle Pliocene (3.7 Ma; Jolly *et al.*, 2016).

Similarly, assuming that the base of the laterally extensive (upper MTD) and associated CLS, mark the onset of the major cooling event at the base of the Gelasian ~2.6 Ma (see Miller *et al.*, 2005; Fig. 8), the base of Unit 7, characterized by erosive CLSs and the onset of strongly reflective seismic packages could be associated with a sea-level fall during the Middle Pleistocene. It was assigned ~?1.9-0.9 Ma on the assumption that it could mark the onset of the high-frequency/high-amplitude sequence cycles (Miller *et al.*, 2005; Fig. 8). The assigned 1.9 Ma seems to agree with a published line located a few kilometers from our study area (see Bellingham *et al.*, 2014).

4.4. 3D seismic geomorphology and depositional architecture

Detailed analysis of interval attribute maps, horizon and time slices focused on Units 5, 6 and 7 (Fig. 5). It allowed us to characterize the depositional architecture within the younger stratigraphic units in detail. RMS amplitude extraction at 3.3 seconds (twt) at the top of parallel, continuous high amplitude seismic packages (C_{bh} facies), revealed the presence of NE-SW trending sinuous channels (Fig. 9A). These channels are characterized by their low amplitudes in

their axes, showing high amplitudes in their overbanks (Fig. 9A). They are interpreted to have incised older amalgamated channel/lobe deposits but were draped with mud during their abandonment (see also Chapin *et al.,* 2002; Jobe *et al.,* 2015). A ~5 m core data retrieved in the FM-1 borehole within the (C_{bh}) facies revealed high net-to-gross channel sand, characterized by blocky gamma-ray log patterns (Fig. 9B)**.** Downstream, a ~2 m core data retrieved in the FM-3ST1 borehole is characterized by interbedded sand and shales that grade downward to dominantly shales characterized by irregular gamma-ray log patterns (Fig. 9B, D). Lateral variation in the gamma-ray log from blocky in the FM-1 borehole to irregular patterns in the FM-3ST1 borehole points to an overall decrease in grain size in this case from the channel axis to overbank deposits characterized by thin interbedded sands and shales.

The RMS amplitude map of the erosive event at the base of Unit 6 revealed the presence of a ~2 km wide, E-W oriented, low-amplitude, moderate sinuosity submarine channel complex (labelled 1; Fig. 10A, B) and three channel levee systems (CLSs labelled 2, 3 and 4), confined to the southern part of the mobile shale zone (Fig. 10 A, B). The main CLS developed tripartite, moderate sinuosity networks with overall E-W paleo-flow direction (Fig. 10A, B). CLS 1 terminated on a moderate amplitude, lobe-like feature (Fig. 10 B). CLSs 3 and 4 are characterized by higher amplitudes and crossed paleo-relief associated with a buried fold/shale-cored anticline (Fig. 10A, B).

RMS amplitude extraction at the base of Unit 7 reveals the presence of a submarine channel complex (SE in Fig. 11B; labelled channel 1), CLSs 2, 3 and 4 (SE in Fig. 11B) and bifurcating, moderate sinuosity CLSs located in the NW corner of the 3D volume (Fig. 11B). The NW CLSs are interpreted as bypass channels that incised older sand-rich amalgamated

451 channels/lobe deposits. The updip continuity of the main submarine channel complex is obscured
452 by mobile shale/erosion (Fig. 11B).

453 Furthermore, the horizon slice at the base of the high reflectivity seismic packages in
454 Unit 7 reveals the presence of erosive submarine channel complex 1 and high sinuosity CLSs 2
455 and 3 (Fig. 12A, B). A seismic line through this channel complex revealed its erosive character
456 and wide U-shaped geometry. This stage marks a significant increase in the width of the channel,
457 the development of higher sinuosity, a northward shift toward the mobile shale zone and overall
458 NE-SW orientation compared to the previous stages (Figs. 10, 11 and12).

459 An RMS amplitude extraction at 1.9 seconds within the high amplitude seismic packages
460 revealed a NE-SW trending, moderate sinuosity submarine channel complex (labeled 1; Fig.
461 13B) and four E-W oriented sinuous CLSs (labelled 2, 3, 4 and 5; Fig. 13B). These channels are
462 all confined to the southern part of the mobile shale zone (Fig. 13). The submarine channel
463 complex 1 captured the CLSs 2 and 3 downslope, where the latter developed abandoned meander
464 loops (Fig. 13). CLS 4 is bordered by a high amplitude sediment wedge interpreted as levee
465 deposits (Fig. 13). The linear, high amplitude channel-like feature located downslope of CLS 4 is
466 interpreted as an avulsion channel (see also Posamentier and Kolla, 2003; Fig. 13).

467 The horizon slice at 1.8 seconds (below the present day seafloor) shows the presence of
468 irregular, low coherent seismic areas in the north, flanked by planar radial discontinuities
469 interpreted as radial faults (Fig. 14A). These low coherent features were interpreted as mobile
470 shales (Figs. 2, 5, 12-14). Linear scars were also observed in a hanging-wall fault block adjacent
471 to the mobile shale zone (Fig. 14). A seismic line through these lineated features revealed
472 coherent to slightly deformed high amplitude seismic packages with a somewhat erosive base.
473 These lineaments were interpreted as scars associated with mobile shale-derived MTDs (Fig.

14D). This MTD shows a lateral distance, area and maximum thickness of ~2.3 km, ~13 km^2 and ~60 m, respectively (Table 1). The presence of an E-W oriented, moderate sinuosity submarine channel complex characterized by rough edges and entrenched CLSs can also be observed on this map (Fig. 14).

5. Discussion

Here, we focus on the sedimentary processes in intraslope basins, interactions between shale tectonics and submarine channel evolution, depositional patterns and their implications for reservoir distribution. We prefer the term 'filled ponded basins' to 'shallow ponded basins' used by Prather *et al.* (2012a) in the description of the depositional architecture in the intraslope basins we studied. We think this term is more appropriate as the 3D block we studied is located in a supply-dominated deep-basin between 900-1,150 m, where deep-water processes dominate, and where the high rate of sediment supply filled the accommodation created by shale tectonics.

5.1 Interaction between shale tectonics and submarine channel complex

Detailed seismic and 3D geomorphological analyses (Fig. 15) revealed that the main submarine channel complex described in Units 6 and 7 (Figs. 10-15) evolved in three stages from the Pliocene to the present day. The evolution of the submarine channel from relatively moderate to high sinuosity over the Pliocene and the Pleistocene could be related to shale tectonics (Figs. 5, 10-15; see also Olusola *et al.*, 2007; Clark and Cartwright, 2012; Jolly *et al.*, 2016; Hansen *et al.*, 2017).

497 During stage 1 (Middle Pliocene-Early Pleistocene), the channel was characterized by
498 narrow morphology, low sinuosity and confined to the south of mobile shale in an E-W
499 orientation (Figs. 10-11, 15). The narrow low sinuosity of the channel during this stage is typical
500 of young submarine channels with a relatively high slope gradient (see also Posamentier and
501 Kolla, 2003; Ferry *et al.*, 2005; Heiniö and Davies, 2007; Jobe *et al.*, 2015; Jolly *et al.*, 2016;
502 Hansen *et al.*, 2017). The E-W orientation of the channel south of the mobile shale zone suggests
503 that the later was active from the Middle Pliocene to the Early Pleistocene, leading to the
504 channel's confinement (Fig. 10-11, 15).

505 Stage 2 (Early to Middle Pleistocene) marks a northward shift of the submarine channel
506 complex toward the mobile shale zone and a transition from an E-W to a NE-SW orientation
507 (Figs. 12, 15). Its higher sinuosity, broad U-shaped morphology are typical features of mature
508 submarine channels with relatively gentle slope gradients (Fig. 12; see also Posamentier and
509 Kolla, 2003; Ferry *et al*., 2005; Jobe *et al.*, 2015; Heiniö and Davies, 2007; Jolly *et al.*, 2016; Qin
510 *et al*., 2016; Hansen *et al.*, 2017). The channel's northward adjustment toward the mobile shale
511 zone (Figs. 12, 15) suggest relative quiescence of mobile shales.

512 Stage 3 (Middle Pleistocene to present day) marks a return of the channel to its original
513 E-W paleo-flow direction, south of the mobile shale zone (Figs. 1D, 14-15). The downward shift
514 of the submarine channel complex suggests that renewed activity of the mobile shale led to the
515 deflection of the submarine channel complex southward away from the mobile shale zone. The
516 presence of NE-SW oriented, high sinuosity submarine channel complexes 1 and 2 at 1.9
517 seconds (twt; middle part of Unit 7; Fig. 13) suggests that shale tectonics and the final southward
518 deflection of the channel complex occurred a little later than the Middle Pleistocene. The
519 presence of mud volcanoes on the present day seafloor supports the ongoing activity of the

520 mobile shale (Fig. 5). The presence of entrenched sinuous channel levee system within a valley
521 (Fig. 14) indicates increasing confinement due to successive erosional and aggradational
522 (depositional) stages (Fig. 13; channel complexes 1 and 2). A large valley containing the
523 channel develops complex geometries as the valley wall becomes unstable (large scars Fig.
524 14A), with the development of inner terraces and a central sinuous channel (labeled in part B).
525 The modification of the channel valley could result from the increasing confinement and focused
526 energy of turbidity currents (see also Gee and Gawthorpe 2007, and others) during their activity.
527 The present day hemipelagic drape (Fig. 14 C) shows that the last channel complex described in
528 this study was not active in the Holocene.
529
530 5.2 Reservoir distribution in filled ponded basins
531
532 Fig. 13 is a detailed example of the recent entrenched channel levee system (CLS) in Unit
533 7. The generally high amplitudes on the upstream bank of channel levee system (e.g. CLS 4; Fig.
534 13) suggest that sand-rich sediment was deposited both in the channel axis and on the overbank.
535 In addition, the chaotic high amplitude reflection packages (HARPs) at the erosional base of the
536 main submarine channel complexes (e.g. Figs. 13, 14; labeled HARPs) are interpreted as coarse
537 grained turbiditic channel fill deposits (after Prather *et al.*, 1998; Heiniö and Davies, 2007;
538 Gamboa and Alves, 2016). However, the occurrence of high RMS amplitudes downstream of the
539 channels (e.g. CLS 4 in Fig.13A, B; labelled avulsion channel) show that turbidity flows
540 periodically spilled sandy deposits on the overbank environment. The presence of high
541 amplitudes associated with the avulsion channel (Fig. 13 A, B) compared to lower amplitudes in
542 the downstream part of the main CLS 4 (Fig. 13), suggests that sand-rich sediment was diverted

543 from the main channel during the avulsion event. Similar observations have been reported in the
544 De Soto Canyon, Gulf of Mexico, where upstream avulsion due to a breached levee resulted in
545 the deposition of the avulsion lobe and concomitant decrease in both water and sediment
546 discharge downstream of the main channel (Posamentier and Kolla, 2003).

547 As a first conclusion, these detailed images of reservoir distribution in Unit 7 are a good
548 analog for the Middle to Late Miocene turbidite deposits described by previous authors as
549 amalgamated channels and overbank deposits (Chapin *et al.,* 2002). However, our study shows
550 that reservoirs topped by hemipelagic layers and/or mud-rich turbidites are Late Oligocene to
551 present day in age (see Figs. 5, 7, 9). Our study also shows that the geometries and the
552 distribution of reservoir could be controlled by both shale tectonics and sediment supply, with
553 prevalence of hemipelagic deposition during the periods of sea level rise (see Figs. 7 and 8).
554 Reservoir facies were confirmed by borehole data (see Fig. 9). Lobe-like deposits (e.g. Fig. 10 B)
555 are generally rare and not discussed further in this paper due to lack of sufficient evidence to
556 fully characterize their architecture.

557

558 5.3 Shale tectonics vs MTD types and distribution:

559

560 Two types of MTDs were recognized based on seismic facies, internal architecture and aerial
561 extent (Figs. 5, 6, 14 D and Table 1): (1) Mobile shale-derived MTDs and (2) regional MTDs.
562 Detailed analysis of kinematic indicators enabled us to infer the source area of the locally
563 derived type 1 MTDs, but the limited size of the 3D volume we studied did not allow us to
564 observe the headwall scars of the type 2 MTDs. However, analysis of their thickness maps
565 helped us to infer their provenance.

566

567 Type 1 (Mobile shale-derived MTDs)

568 The type 1 MTDs described in seismic Unit 7 are thin and laterally confined adjacent to
569 mobile shales (Fig. 14. D; Table 1). Their strong reflectivity distinguishes them from the type 2
570 MTDs, and their overall coherent internal architecture indicates that they are close to their source
571 area (mobile shales).

572 Type 2 (Regional MTDs)

573 The type 2 MTDs described in Unit 6 (labelled lower, middle and upper MTDs; Figs. 5,
574 6; Table 1) are characterized by thick, chaotic, discontinuous low amplitude/transparent seismic
575 packages that are bounded at the base by laterally extensive erosional scours. Their thick, lateral
576 distribution, low amplitudes and chaotic internal architecture indicate that they were reworked
577 far from their source areas (shelf-margin/upper slope).

578 The distribution of the regional MTDs could be controlled by general slope (Fig. 6), syn-
579 depositional faulting (Fig. 6 B) and differential compaction/cementation in the underlying
580 substratum (Fig. 6 D).

581 The lower MTD increases in thickness from the NE downslope to the SW suggesting
582 possible source area upslope (Fig. 6C; see also Alves *et al.*, 2009). However, the local increase in
583 MTD thickness on both side of CLSs (Figs. 5, 6C, G), suggest that the degree of
584 compaction/cementation in the underlying CLSs could be a controlling factor at local scale. The
585 differential erosion in sandy CLSs and muddy deposits could also explain the observed variation
586 in thickness of the lower MTD (see erosional truncations at its base, Fig. 6 G).

587 We observed a NE-SW decrease in thickness of the middle MTD downstream (6B, F)
588 due to its confinement within fault bounded accommodation (Hanging-Wall; HW; Fig. 6F). This

589 observation suggests that the deposition of MTD in the intraslope basins of the Niger Delta was
590 controlled by syn-depositional normal faults (P, Q? Fig. 6 F) that were active during the
591 emplacement of MTD (Fig. 6B, F).

592 The thickness of the upper MTD increases downstream and was locally controlled by the
593 degree of compaction in the underlying CLSs (Fig. 6A). The overall downstream increase in
594 thickness of this MTD suggests a response to regional accommodation development (see also
595 Alves *et al.*, 2009). The foregoing observations strongly suggest that the type 2 MTDs originate
596 from shelf-margin and/or upper slope.

597

598 5.4 Control of depositional systems in filled ponded basins:

599

600 Our results show that the depositional architecture of the filled ponded basins in the
601 western Niger Delta is controlled by shale tectonics, sediment supply and eustasy.

602 At local scale, basin tectonics is associated with mobile shale deformation and syn-
603 depositional faults, controlling submarine channel morphology and depositional patterns in these
604 filled ponded basins. Inferred high uplift/subsidence rates driven by the mobile shale in the
605 Middle Pliocene and Early Pleistocene resulted in high slope gradients characterized by
606 erosionally confined channels with low sinuosity (e.g. Figs. 10B, C, D; 11 A, C). However,
607 relative quiescence and/or low subsidence/uplift rates from the Early to Middle Pleistocene
608 resulted in more mature CLSs characterized by complex terraces, overbank deposits and channel
609 avulsion (e.g. Fig. 13). The erosional nature of the main submarine channel complex during
610 mobile shale deformation suggest that a dynamic equilibrium was maintained between changing
611 local slope gradients and sedimentation rates (see also Adeogba *et al.*, 2005; Clark and

Cartwright, 2012; Jolly *et al.*, 2016; Hansen *et al.*, 2017). Similar observations have been made in the adjacent lower Congo Basin (Ferry *et al.*, 2005).

In addition, the control of the distribution of MTDs by syn-depositional faults suggests that mass-wasting was coeval with the growing faults. Equivalent observations have been reported in the lower Congo Basin (Ferry *et al.*, 2005).

At a basin scale, the depositional sequence is characterized by a succession of MTDs and turbidite deposits topped by hemipelagic layers (see Fig. 6G). Moreover, the Plio-Pleistocene sedimentary records show that eustasy and sediment supply could control the depositional architecture at regional scale (e.g. Figs. 5, 6E, G, H; 10-13C). The absence of thick hemipelagic drape above the older submarine channel complex (e.g. CLS 1 Fig 10 C, D) suggests that this hemipelagic drape could have been eroded during stage 1 of the submarine channel complexes or that the former was below resolution. However, the presence of a thick hemipelagic layer above the present day submarine channel complex (just below the present day seafloor; Figs. 5, 10 C, D; 12-14 C) indicates that it was draped and abandoned during the last postglacial sea level rise. These observations suggest that channel complexes were most active during the low eustatic sea level but that hemipelagic sedimentation prevailed during high eustatic sea level.

Conclusions

The Neogene stratigraphy of the western Niger Delta's slope is characterized by seven major seismic units dated as Chattian, Burdigalian, Serravallian, Tortonian, Middle Pliocene, Middle Pleistocene and present day. Major changes in the sedimentary record occurred in the Pliocene-Pleistocene, characterized by erosional MTDs, turbidites and channel levee systems

draped by hemipelagites. In the Plio-Pleistocene upper sequences, we observed changes in the morphology of submarine channel complexes over time (low sinuosity/highly erosive versus high sinuosity/depositional) that were controlled by the interaction between shale tectonics (creating accommodation, and controlling the seafloor profile) and sediment supply.

Younger sequences of the Niger Delta upper slope could be a good analog for sedimentary processes in intraslope basins; at the margin scale, depositional architecture in the filled ponded basins on the upper slope of the western Niger Delta is controlled by the interaction between local basin tectonics, eustasy and sediment supply. Reservoir facies are characterized by amalgamated channel fills and overbank deposits. Periodic levee breaching by high-energy turbidity currents results in channel avulsion and diversion of sand-rich sediments downstream of avulsion channels. Our detailed analysis of the depositional architecture of the Tortonian and Plio-Pleistocene sedimentary units provides useful analog for deeper exploration of the older stratigraphic units.

Acknowledgments

The authors would like to thank the Federal Republic of Nigeria for funding the PhD of Kelvin Ikenna Chima under the auspices of the Petroleum Technology Development Fund (PTDF) Scholarship Scheme. We are indebted to Shell Nigeria for providing data and permission to publish this study. The first author thanks the management and staff of Alex Ekwueme Federal University Nudfu-Alike Ikwo (AE-FUNAI), Ebonyi State, Nigeria for their continued support and encouragement. Many thanks to Olusegun Obilaja, Adekemi Afolayan, Babatope Atitebi, Richard Streatfield and Timi Tralagba for their invaluable support with data. The *Institute des Sciences de la Terre* (ISTeP), Paris provided the computer workstation used in data analysis and

interpretation. Many thanks to Schlumberger for providing the Petrel (TM) Software used in 3D data interpretation. Many thanks to Dia Ninkabou, Quentin Soulet, Douglas Lisboa (Sorbonne University) and David Anomneze (Camac Petroleum, Nigeria) for software support. This paper benefited from insightful discussion with Miguel Mora-Glukstad (Shell Nigeria). Mark Newall, Celestine Ugwu, Otuka Umahi, Adebukonla Kalejaiye, Segun Akinrolabu, Obobi Onwuka, Ifekelunma Umeogu, Jerome Odiwanor and Jude Omuije (Shell Nigeria) are thanked for organizing a discussion session during manuscript drafting. Bilal Haq provided insightful review comments on the first draft. Marzia Rovere and Kamaldeen Olakunle Omosanya are thanked for their high quality and constructive review comments/suggestions, which greatly improved the quality of this paper. Daphne Goodfellow proof read the revised manuscript. We thank the invited editor Tiago M. Alves not only for granting us sufficient time to make revisions, but also for pointing out subtle errors in the final submission.

References

Adeogba, A.A., McHargue, T.R., Graham, S.A., 2005. Transient fan architecture and depositional controls from near-surface 3D seismic data, Niger Delta continental slope. AAPG Bulletin 89, 627–643.

Agnini, C., Fornaciari, E., Raffi, I., Catanzariti, R., Pälike, H., Backman, J., Rio, D., 2014. Biozonation and biochronology of Paleogene calcareous nannofossils from low and middle latitudes. Newsletters on Stratigraphy 47, 131–181.https://doi.org/10.1127/0078-0421/2014/0042

Allen, J. R. L., 1965. Late Quaternary Niger Delta and adjacent areas: sedimentary environments and lithofacies. AAPG Bulletin 49, 547-600.

Alves, T.M., Cartwright, J., Davies, R., 2009. Faulting of salt-withdrawal basins during early halokinesis: effects on the Palaeogene Rio Doce Canyons System (EspiritoSanto Basin, Brazil). AAPG Bulletin 93, 617-652.

Alves, T.M., Lourenço, S.D.N., 2010. Geomorphologic features related to gravitational collapse:

submarine landsliding to lateral spreading on a Late MioceneeQuaternary slope (SE Crete, eastern Mediterranean). Geomorphology 123, (1-2), 13-33, http://dx.doi.org/10.1016/j.geomorph.2010.04.030

Alves, T. M., 2015. Submarine slide blocks and associated soft-sediment deformation in deep-water basins: A review. Marine and Petroleum Geology 67, 262-285.

Anthonissen, D.E., Ogg, J.G., 2012. Cenozoic and Cretaceous Biochronology of Planktonic Foraminifera and Calcareous Nannofossils, in: The Geologic Time Scale. Elsevier, pp. 1083-1127. https://doi.org/10.1106/B978-0-444-59425-9-15003

Avbovbo, A. A., 1978, Tertiary lithostratigraphy of the Niger Delta: AAPG Bulletin, 62, 295–300.

Backman, J., Raffi, I., Rio, D., Fornaciari, E., Pälike, H., 2012. Biozonation and biochronology of Miocene through Pleistocene calcareous nannofossils from low and middle latitudes. Newsletters on Stratigraphy 45, 221–244. https://doi.org/10.1127/0078-0421/2012/0022

Bellingham, P., Connors, C., Haworth, R., Barbara, R., Danforth, Al., 2014. The Deep-water Niger Delta: An Underexplored World Class Petroleum Province. Petroleum Geoscience Magazine 11, 1-9.

Benjamin, U. K., Huuse, M., Hodgetts, D., 2015. Canyon-confined pockmarks on the western Niger Delta slope. Journal of African earth Sciences 107, 15-27.

Benjamin, U. K., Huuse, M., 2017. Seafloor and buried mounds on the western Niger Delta Slope.
Marine and Petroleum Geology, 83, 158-173.

Bilotti, F. D., J. H. Shaw, R. M. Cupich, and R. M. Lakings, 2005. Detachment fold, Niger Delta, in J. H. Shaw, C. Connors, and J. Suppe, eds., Seismic interpretation of contractional fault related folds: AAPG Studies in Geology 53, 103– 104.

Booth, J. R., Dean, M. C., DuVernay III, A. 2003. E., Styzen, M. J Paleo-bathymetric controls on stratigraphic architecture and reservoir development of confined fans in the Auger Basin: central Gulf of Mexico slope. Journal of Marineand Petroleum Geology 20, 563-586. doi:10.1016/i.marpetgeo.2003.03.008.

Burke, K., 1972. Longshore drift, submarine canyons and submarine fans in development of Niger Delta: AAPG, Bulletin, 56, 1975-1983.

Brown, A.R., 1999. Interpretation of Three-dimensional Seismic Data. fifth ed. American Association of Petroleum Geologists, Oklahoma

Brownfield, M. E., 2016. Assessment of undiscovered oil and gas resources of the Niger Delta Province, Nigeria and Cameroon, Africa, in Brownfield, M. E., compiler, Geologic assessment of undiscovered hydrocarbon resources of Sub-Saharan Africa. U.S.

Geological Survey Digital Data Series 69–GG, chap. 5, 20. http://dx.doi.org/10.3133/ds69GG.

Catuneanu, 2006. Principles of sequence stratigraphy, first edition, the Netherlands.

Chapman, M. R., chepstow-Lusty, A. J., 1997. Late Pliocene climate change and the global extinction of the discoasters: an independent assessment using oxygen isotope records. Paleogeography, Paleoclimatology, Plaleoecology 134, 109-125.

Chapin, M., Swinburn, P., van der Weiden, R., Skaloud, D., Adesanya, S., Stevens, D., Varley, C., Wilkie, J., Brentjens, E., Blaauw, M., 2002. Integrated seismic and subsurface characterization of Bonga Field, offshore Nigeria. The Leading Edge 21, 1125–113.

Chardon, D., Grimaud, J.-L., Rouby, D., Beauvais, A., Christophoul, F., 2016. Stabilization of large drainage basins over geological time scales: Cenozoic West Africa, hot spot swell growth, and the Niger River: hot spot swell growth and Niger River. Geochemistry, Geophysics, Geosystems 17, 1164–1181.

Chopra, S., Marfurt, K.J., 2007. Seismic attributes for prospect identification and reservoir characterization. Tulsa, Oklahoma, 457.

Clark, I. R. and Cartwright, J. A., 2012. Interactions between coeval sedimentations and deformation from the Niger Delta deep-water fold belt. SEPM 3, 243-267.

Cobbold, P. R., Clark., B. J., and Loseth, H., 2009. Structural consequences of fluid overpressure and seepage forces in the outer thrust belt of the Niger Delta. EAGE 15, 3-15.

Cohen, H.A., McClay, K., 1996. Sedimentation and shale tectonics of the northwestern Niger Delta front. Marine and Petroleum Geology 13, 313–328.

Connors, C. D., Denson, D. B., Kristiansen, G. and Angstadt, D. M., 1998. Compressive anticlines of the mid-outer slope, central Niger Delta (abs.) AAPG Bulletin, 82, 1903.

Corredor, F., Shaw, J.H., Bilotti, F., 2005. Structural styles in the deep-water fold and thrust belts of the Niger Delta. AAPG Bulletin 89, 753780. https://doi.org/10.1306/02170504074

Damuth, J. E., 1994. Neogene gravity tectonics and depositional processes on the deep Niger Delta continental margin: Marine and Petroleum Geology, 11, 320–346.

DeJong, K.A., Scholten, R., 1973. Gravity and Tectonics. John Wiley, New York.

Doust, H., and E. Omatsola, 1990. Niger Delta, in J. D. Edwards and P. A. Santogrossi, (eds.); Divergent passive margin basins. AAPG Bulletin 48, 239-248.

Evamy, B.D., Haremboure, J., Kammerling, R., Knaap, W.A., Molloy, F.A., and Rowlands, P.H., 1978. Hydrocarbon habitat of Tertiary Niger Delta. AAPG Bulletin 62, 1-39.

Ferry, J. N., Mulder, J., Praize, O., and Raillad, S., 2005. The concept of equilibrium profile in Deep-water turbidite systems: effects of local physiographic changes on the natural sedimentary process and geometries of deposits. The Geological Society of London 244, 181-193.

Frey Martinez, J., Cartwright, J., Hall, B., 2005. 3D seismic interpretation of slump complexes: examples from the continental margin of Israel. Basin Research 17, 83-108.

Gamberi, F., Rovere, M., Marani, M.P., 2011. Mass-transport complex evolution in a tectonically active margin (Gioia Basin, Southeastern Tyrrhenian Sea). Marine Geology 279, (1-4), 98-110. 10.1016/j.margeo.2010.10.015

Gamberi, F., M. Rovere, Marani, M.P., Dykstra, M., 2015. Modern deep-sea fan facies development along a tectonically active margin. *Geosphere*, 11, 307-319. 10.1130/GES01030

Gamboa, D., Alves, T.M., 2016. Classifications of submarine confluences and implications for intra-canyon sediment distribution. GSA Annual Meeting, Denver, 2016. 10.1130/abs/2016AM-281380

Gee, J. M. R., Gawthorpe, R. L., 2007. Early Evolution of submarine channels offshore Angola revealed by three-dimensional seismic data. The Geological Society of London Special Publication, 277; 223-236.`

Gorini, C., Haq, B.U., dos Reis, A.T., Silva, C.G., Cruz, A.M., Soares, E., and Grangeon, D., 2014. Late Neogene sequence stratigraphic evolution of the Foz do Amazonas Basin, Brazil. Terra Nova, 26, (3), 179–185. https://doi.org/10.1111/ter.12083

Graue, K., 2000. Mud volcanoes in deep-water Nigeria. Marine and Petroleum Geology 17, 959–974. https://doi.org/10.1016/S0264-8172(00)00016-7

Grimaud, J.-L., Rouby, D., Chardon, D., Beauvais, A., 2017. Cenozoic sediment budget of West Africa and the Niger delta. Basin Research, 1-18.

Hansen, L., Janocko, M., Kane, I., Kneller, B., 2017. Submarine channel evolution, terrace development, and preservation of intra-channel thin-bedded turbidites: Mahin and Avon channels, offshore Nigeria. Marine Geology 383, 146–167. https://doi.org/10.1016/j.margeo.2016.11.011

Haq, B.U., Hardenbol, J., Vail, P.R., 1987. Chronology of fluctuating sea levels since the triassic. Science, 235, 1156–1167.

Heiniö, P., Davies, R. J., 2007. Knickpoint migration in submarine channels in response to fold growth, western Niger Delta. Marine and Petroleum Geology 24, 434-449. doi.org/10.1016/j.marpetgeo.2006.09.002

Jobe, Z.R., Sylvester, Z., Parker, A.O., Howes, N., Slowey, N., Pirmez, C., 2015. Rapid adjustment of submarine channelarchitecture to changes in sediment supply. Journal of Sedimentary Research 85, 729–753.

Jolly, B.A., Lonergan, L., Whittaker, A.C., 2016. Growth history of fault-related folds and interaction with seabed channels in the toe-thrust region of the deep-water Niger Delta. Marine and Petroleum Geology 70, 58–76.

Kneller, B., McCaffrey, W.,1999. Depositional effects of flow nonuniformity and stratification within turbidity currents approaching a bounding slope: deflection, reflection and facies variation. Journal of Sedimentary Research, 69(5), 980-991.

Masson, D.G., Watts, A.B., Gee, M.J.R., Urgeles, R., Mitchell, N.C., Le Bas, T.P., Canals, M., 2002. Slope failures on the flanks of the western Canary Islands.Earth-Science Reviews 57 (1-2), 1-35

Miller, K.G., Kominz, M.A., Browning, J.V., Wright, J.D., Mountain, G.S., Katz, M.E., Sugarman, P.J., Cramer, B.S., Christie-Blick, N., Pekar, S.F., 2005. The Phanerozoic Record of Global Sea Level Change. Science Magazine 310, 1293-1298.

Mitchum, R.M.,Vail, P.R., 1977. Seismic Stratigraphy and Global Changes of Sea Level, Part 7: Seismic Stratigraphic Interpretation Procedure: Seismic Stratigraphy: Applications to Hydrocarbon Exploration. AAPG Memoir 26, 135–143.

Morgan, R., 2004. Structural controls on the positioning of submarine channels on the lower slopes of the Niger Delta, in: Davies, R.J., Cartwright, J., Stewart, S.A., Underhill, J.R., Lappin, M. (Eds.), 3D Seismic Technology: Application to the Exploration of Sedimentary Basins. Geological Society of London Memoir 29, 45-51

Morley, C. K., and Guerin, G., 1996. Comparison of gravity-driven deformation styles and behavior associated with mobile shales and salt. Tectonics 15, 1155-1170.

Morley, C. K., King, R., Hillis, R., Tingay, M., Backe, G., 2011. Deep-water fold and thrust belt classification, tectonics, structure and hydrocarbon perspectivity. Earth Sciences Reviews 104, 41-91.

Olusola, B., Hurley, N., McHargue, T., 2007. Effect of Growing Structures on Stratigraphic Evolution, Channel Architecture, and Submarine Fan Distribution, Niger Delta, West
Africa. AAPG Conference Proceedings, California.

Omosanya, K.O., Alves, T. M., 2013. A 3-dimensional seismic method to assess the provenance of Mass-Transport Deposits (MTDs) on salt-rich continental slopes (Espírito Santo Basin, SE Brazil). Marine and Petroleum 44, 223-239.

Omosanya, K. O., Harishidayat, D., 2019. Seismic geomorphology of Cenozoic slope deposits and deltaic clinoforms in the Great South Basin (GSB) offshore New Zealand. Geo-Marine Letters. https://doi.org/10.1007/s00367-018-00558-8

Prather, B. E. 2000. Calibration and visualization of depositional process models for above-grade slopes: a case study from the Gulf of Mexico. Marine and Petroleum Geology, 17(5), 619-638.

Prather, B. E., 2003. Controls on reservoir distribution, architecture ad stratigraphic trapping in slope settings. Marine and Petroleum 20, 529-545.

Prather, B.E., Pirmez, C., Sylvester, Z., and Prather, D. S., 2012a. Stratigraphic Response to Evolving Geomorphology in a Submarine Apron Perched on the Upper Niger Delta Slope. SEPM 99, 145-161.

Posamentier, H.W., Kolla, V., 2003. Seismic geomorphology and stratigraphy of depositional elements in deep-water settings. Journal of sedimentary research 73, 367–388.

Qin, Y., Alves, T. M., Constantine, J., and Gamboa, D., 2016. Quantitative seismic geomorphology of a submarine channel system in SE Brazil (Espirito Santo Basin): Scale comparison with other submarine channel systems. Marine and Petroleum Geology 78, 455-473. https://doi.org/10.1016/j.marpetgeo.2016.09.024

Raffi, I., Agnini, C., Backman, J., Catanzariti, R., and Pälike, H., 2016. A Cenozoic calcareous nannofossil biozonation from low and middle latitudes: A synthesis.

Ramberg, 1981. Gravity, deformation and the Earth's crust in theory, experiments and geological application 2nd Edition, Academic Press, London.

Rouby, D., Nalpas, T., Jermannaud, P., Robin, C., Guillocheau, F., Raillard, S., 2011. Gravity driven deformation controlled by the migration of the delta front: The Plio-Pleistocene of the Eastern Niger Delta. Tectonophysics 513, 54–67. https://doi.org/10.1130/GEOSO1426.1

Richardson S.E.J, Davies R. J, Allen M.B., Grant S.F., 2011 Structure and evolution of mass transport deposits in the South Caspian Basin, Azerbaijan. Basin Research 23:702-719.

Rovere, M., Gamberi, F., Mercorella, A., leidi, Elisa., 2014. Geomorphometry of a submarine mass-transport complex and relationships with active faults in a rapidly uplifting margin (Gioia Basin, NE Sicily margin). Marine Geology. http://dx.doi.org/10.1016/j.margeo.2013.06.003

Short, K. C., Stauble, A. J. 1967. Outline of geology of Niger Delta: AAPG Bulletin, 51, 761–779.

Taner, M.T., Schuelke, J.S., O'Doherty, R., Baysal, E., 1994. Seismic attributes revisited. In: SEG technical program expanded abstracts 1994. https://doi.org/10.1190/1.1822709.

Tuttle, W.L.M, Brownfield, E.M. and Charpentier, R.R. 1999. The Niger Delta Petroleum System. Chapter A: Tertiary Niger Delta (Akata-Agbada) Petroleum System, Niger Delta Province, Nigeria, Cameroon and Equatorial Guinea, Africa. USGS, Open File Report. 99-50-H, 4-44.

Wiener, R.W., Mann, M. G., Angelich, M. T., Molyneux, J. B., 2010. Mobile shale in the Niger Delta: Characteristics, structure, and evolution. AAPG, 93, 145-161.

Whiteman, A.J., 1982. Nigeria: Its petroleum geology resources and potential Parts II and I: Edinburgh/London, Graham and Trotman, 39.

Wu, S., Bally, A. W 2000. Slope tectonics. Comparisons and contrasts of structural styles of salt and shale tectonics of the northern Gulf of Mexico with shale tectonics of offshore Nigeria in Gulf of Guinea, in W. Mohriak and M. Talwani, eds., Atlantic rifts and continental margins: Washington, D.C., American Geophysical Union, 151-172.

ACCEPTED MANUSCRIPT

ACCEPTED MANUSCRIPT

Table 1: Summary of statistical measurements on MTDs

Name	Length (m)	Thickness (m)	Area (km^2)
Mud-derived MTD	2.3	75	13
Upper MTD	12	205	187
Middle MTD	6-8	246	175
Lower MTD	3-5	148	155

ACCEPTED MANUSCRIPT

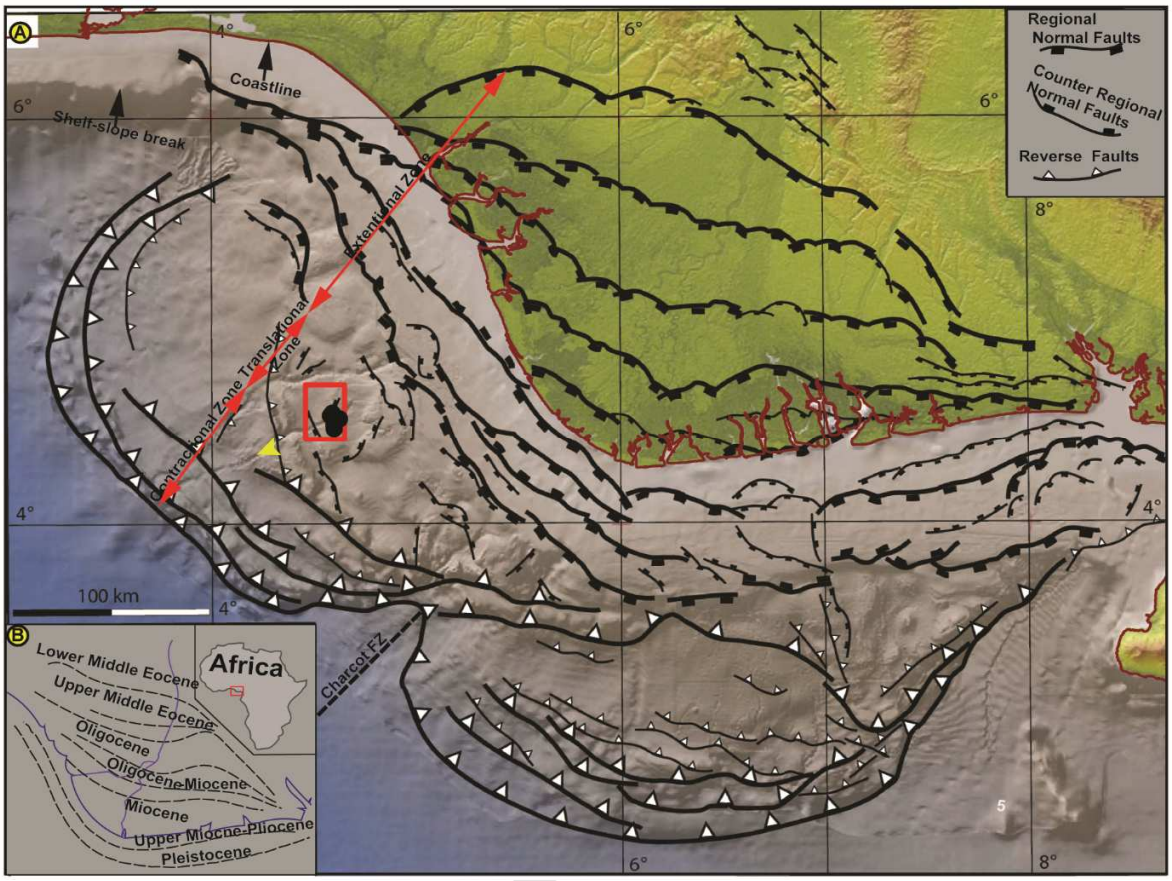


Fig. 1. A: Superposed relief and bathymetric map of the Niger Delta showing the extensional, translational and compressional zones. B: Schematic map showing progradation of the delta from the Late Eocene to the present day. The red box in inset map B shows the location of the Niger Delta in the Gulf of Guinea. Red box and black circles in A show the limit of the 3-D block we studied and the locations of the boreholes, respectively. Yellow arrow points to the downstream section of the submarine channel complex that crossed the study area. A, B modified after (Rouby *et al.*, 2011).

ACCEPTED

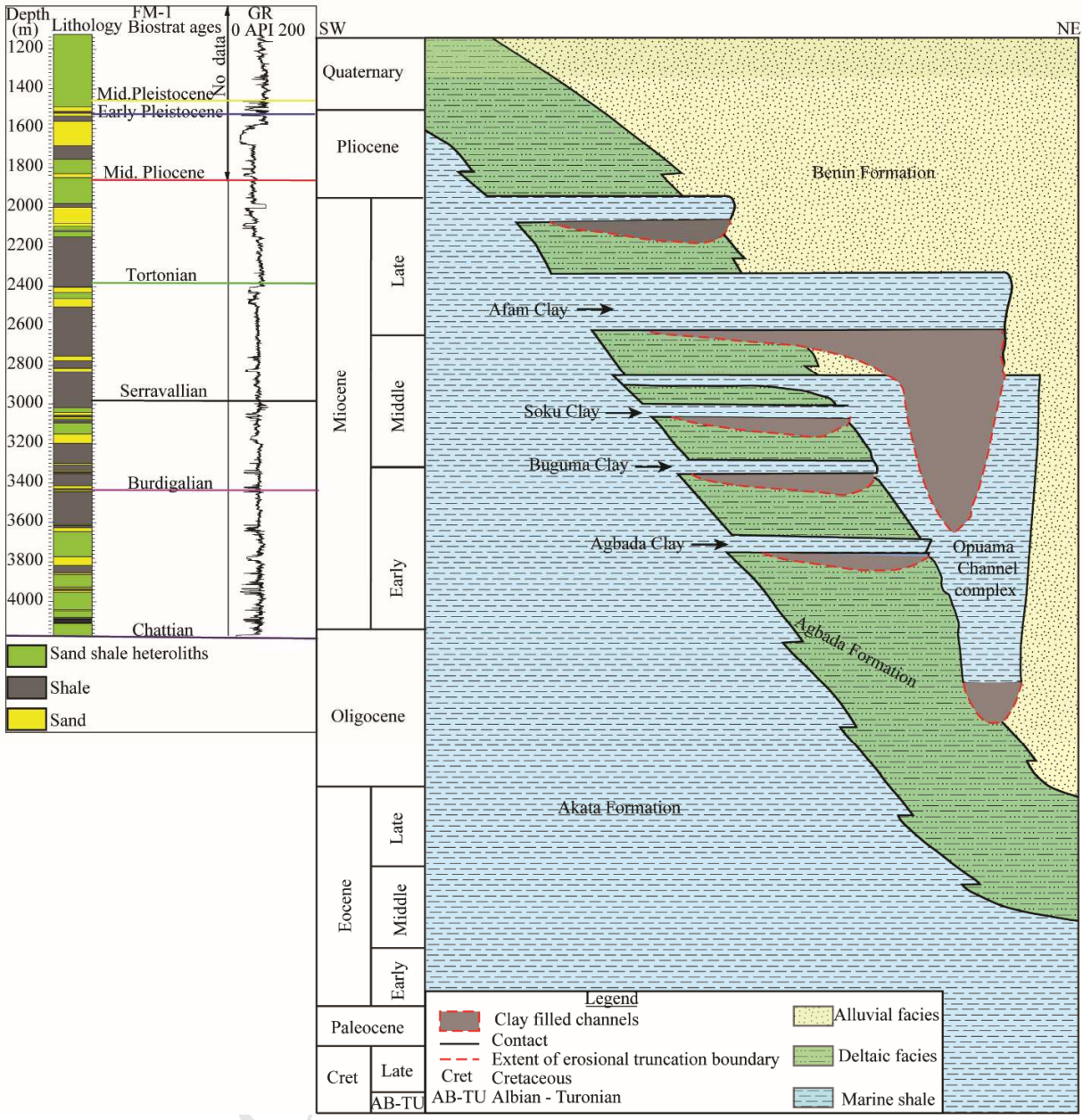


Fig. 2. Schematic diagram (not drawn to scale) of the three lithostratigraphic units underlying the Niger Delta (redrawn after Brownfield, 2016, on the right). Representative deep borehole (FM-1 well) that penetrated more than 4 km into the deeper Neogene sedimentary records in the Akata Formation and the bio-chronostratigraphycally dated intervals in this study (on the left).

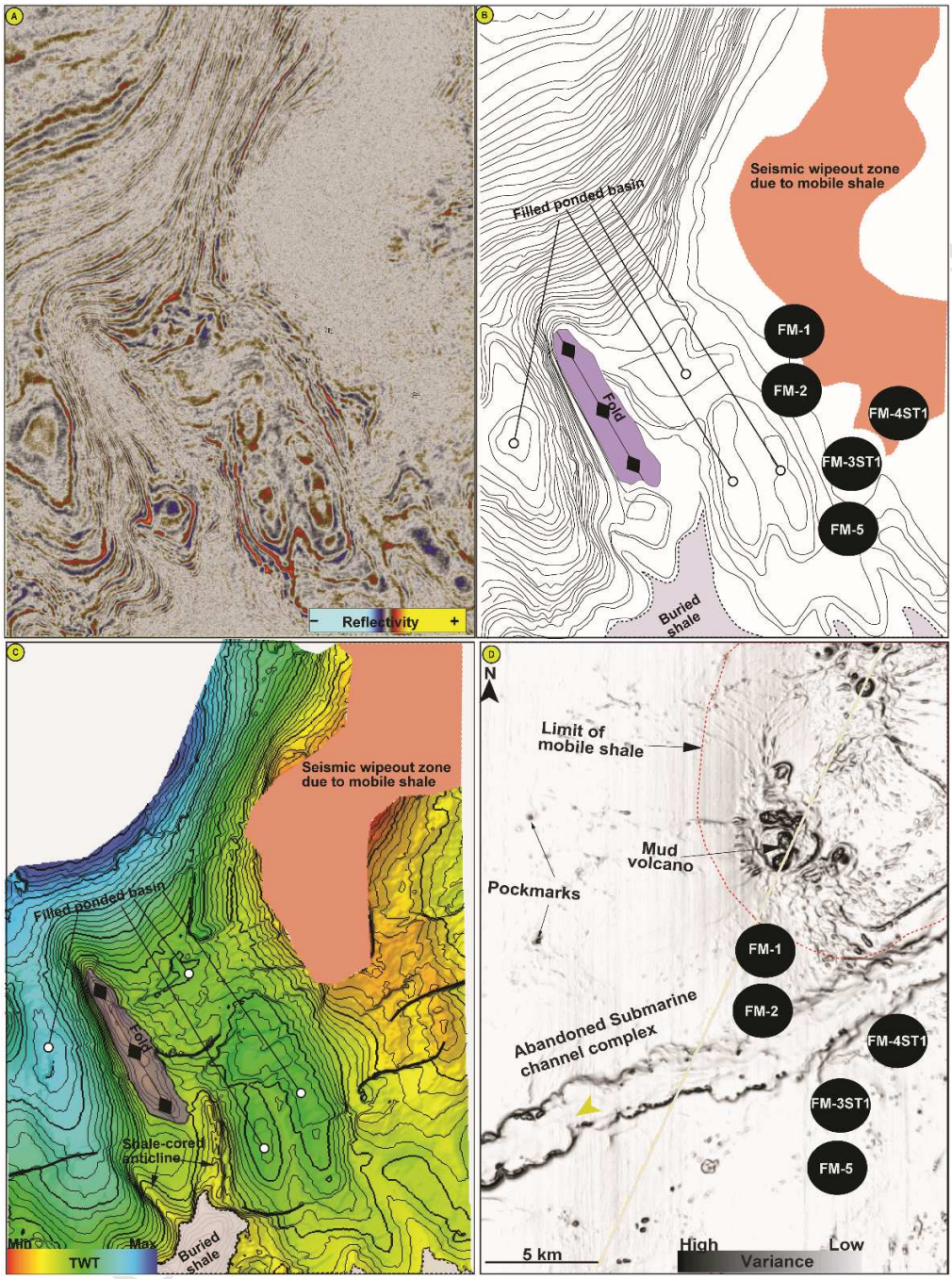


Fig. 3. Physiography of the study area. A, B: Uninterpreted and uninterpreted time slice (at 4.9 seconds twt) showing mobile shales and filled-ponded basins in the block studied. C: Time-structure map near the level of time slice illustrating the same features as in panels A and B. D: Variance attribute map of the seabed showing the presence of mud volcanoes and submarine channel complex. Black dots show the location of the boreholes.

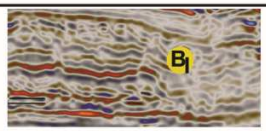
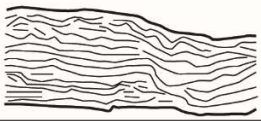
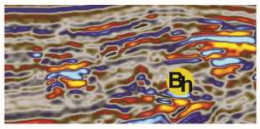
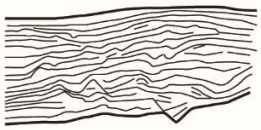
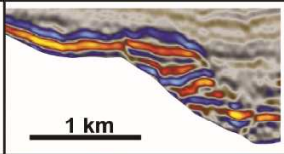
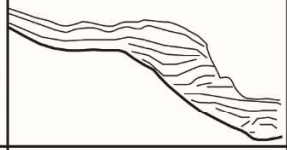
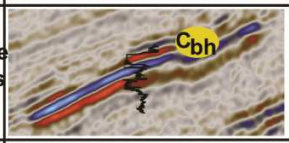
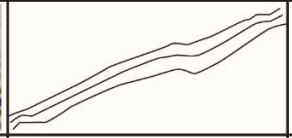
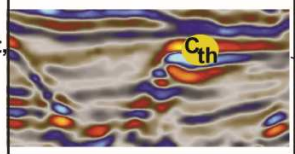
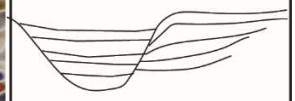
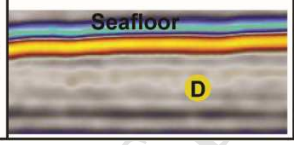
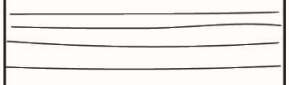
Prather *et al.* (1998);Basin floor/slope depositional environments	Seismic facies	Line drawing	Depositional Architecture
Mass-flow deposits with variable lithology			MTD
Turbidite feeder channel systems, amalgamated channel sands			Turbidite feeder channels
Submarine slide /slumps			Slide blocks/slumps
Basin-floor and slope, submarine fan complexes with sand sheets and levees			Amalgamated channels/ lobe deposits
Fine-grained suspension fallout, Muddy/overbank turbidites and hemipelagic drapes on slopes			Channel fill and levees/ overbank deposits
Muddy turbidites to condensed section and hemipelagic drape			Hemipelagic drape

Fig. 4: Overview of the seismic facies observed in this study, corresponding line drawings and interpretations of the depositional environment.

ACCEPTED

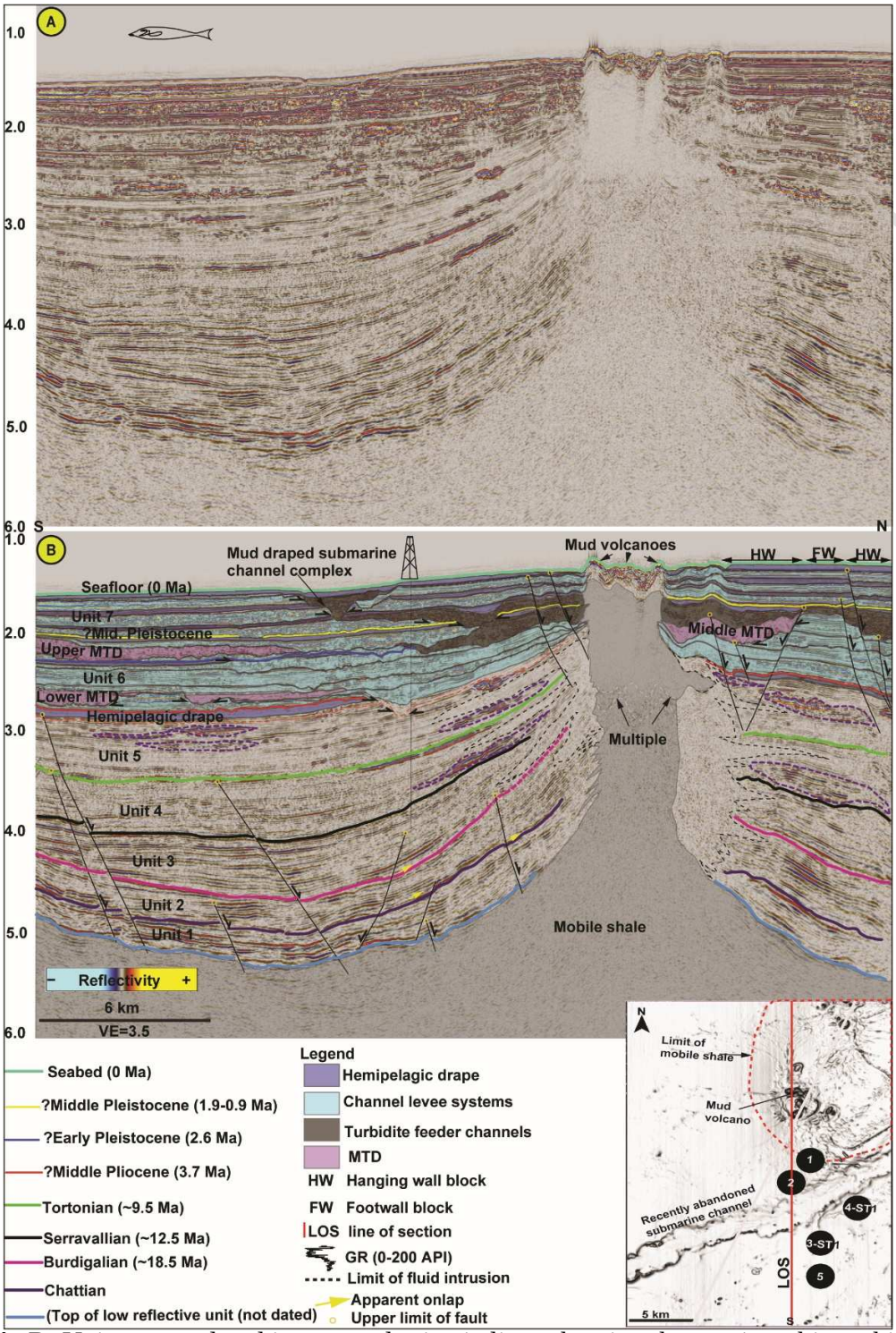


Fig. 5. A, B: Uninterpreted and interpreted seismic lines showing the stratigraphic architecture of the study area. Note the lateral discontinuities (erosional truncations) and the juxtaposition of different seismic facies.

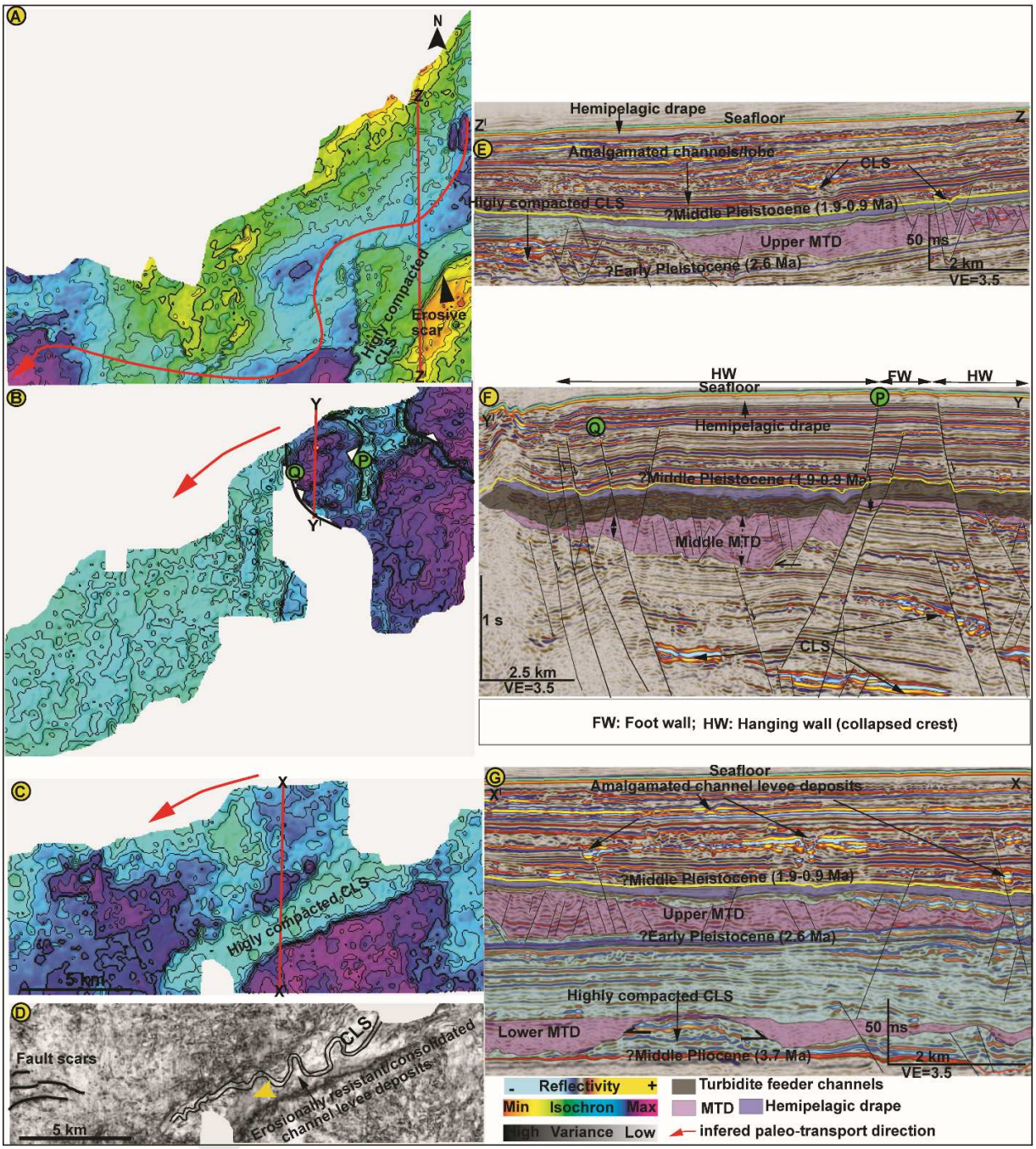


Fig. 6. A, B, C: Isochron maps of the lower, middle and upper MTD showing respective spatial variations in sediment thickness. D: Horizon slice at the top of the amalgamated channel levee deposits underlying the lower MTD showing the presence of sinuous channel. E-G: Seismic lines illustrating the architecture of the MTDs. Variations in the thickness of the middle MTD on the

footwall and hanging wall blocks are indicated by double-headed arrows (panel F). See text for detailed explanation.

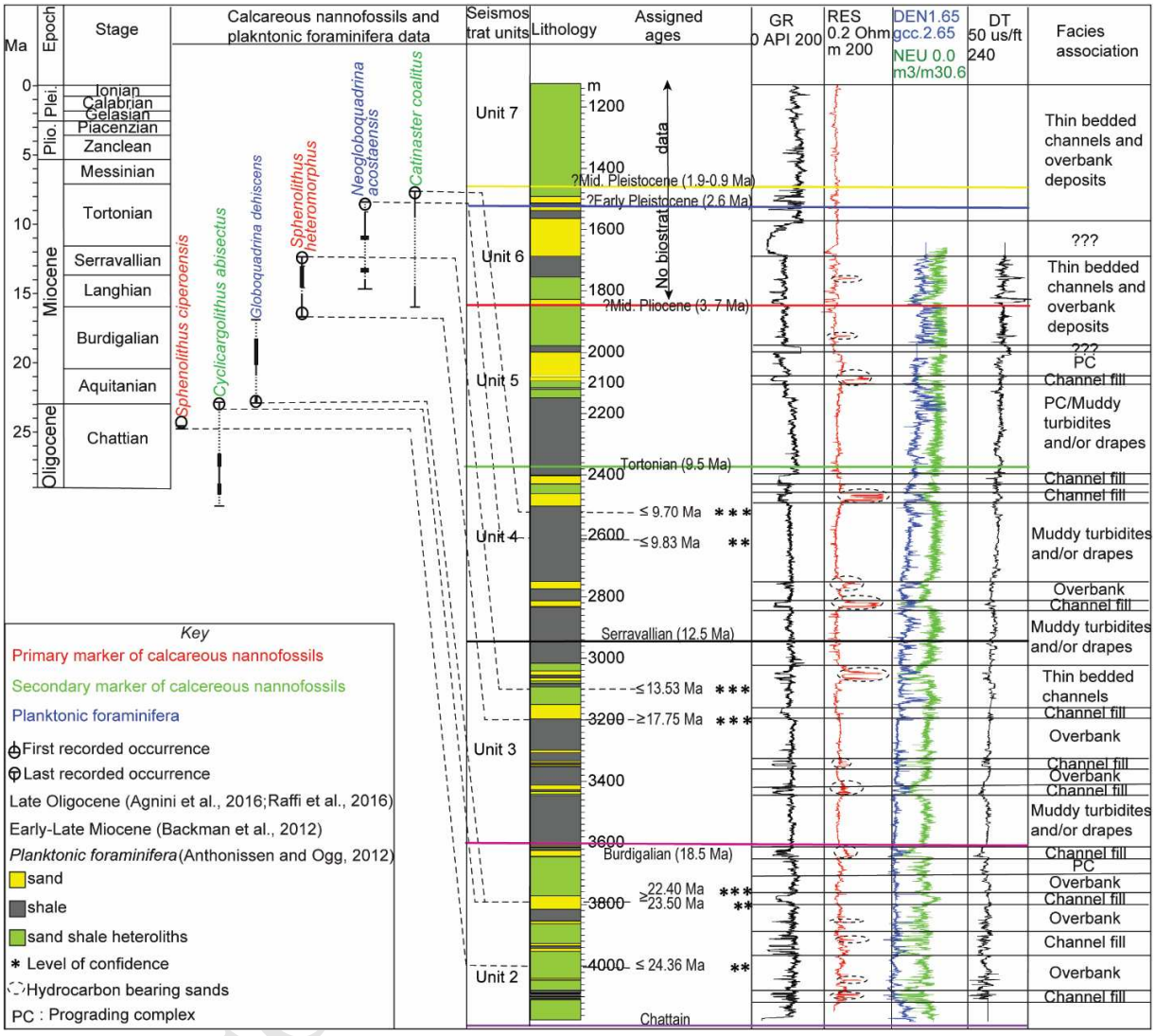


Fig. 7: Representative borehole (FM-1 well) drilled to a total depth of 4.15 km down to the Neogene series. The identified fossil markers, data and estimated ages are shown on the left. The well logs used for lithology, facies and depositional environment analysis are shown on the right. Note the vertical succession of facies from channel axis, overbank and/or hemipelagic deposits. See text for a detailed explanation.

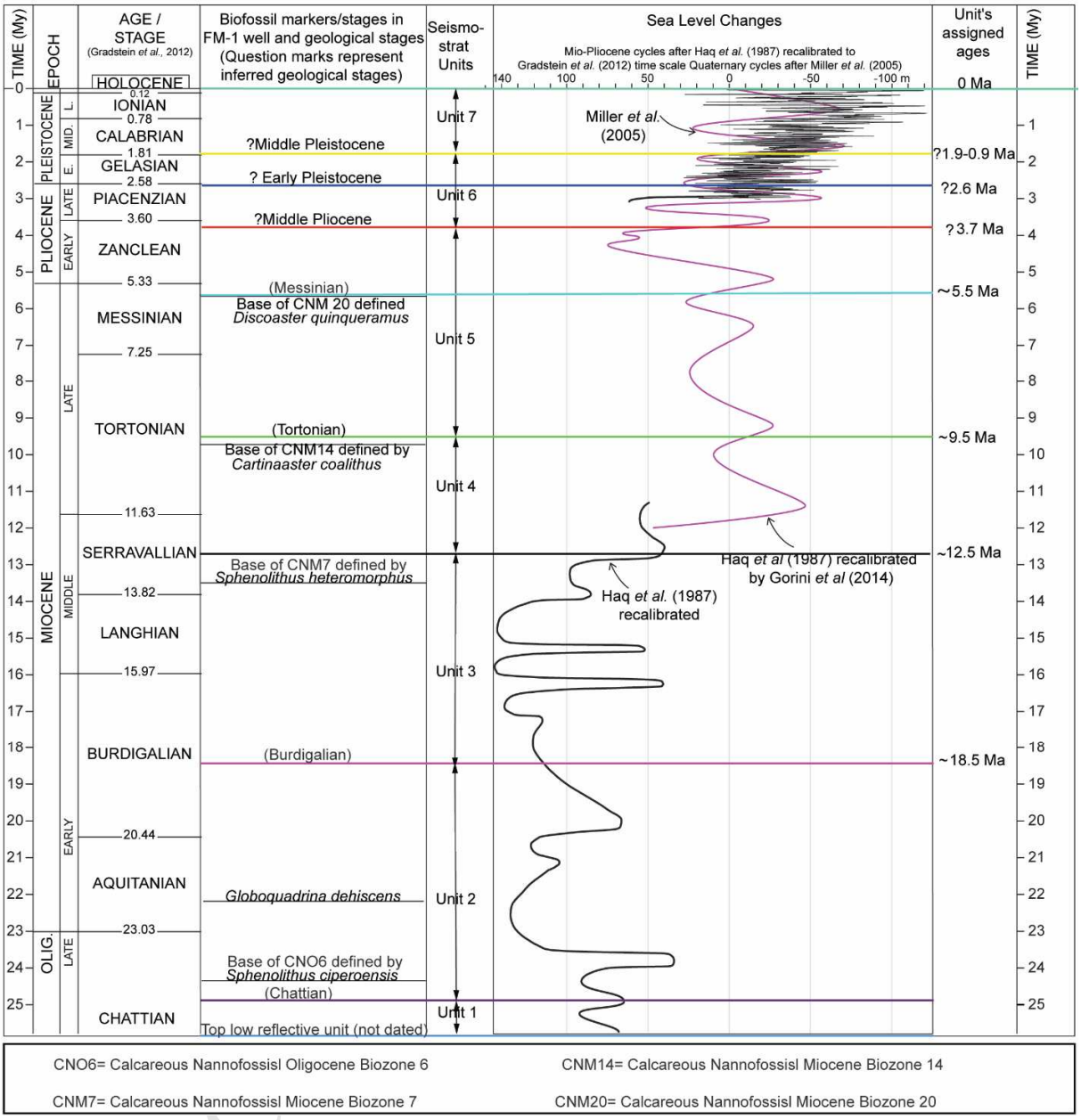


Fig. 8: Chronostratigraphic chart showing standard stages, long-term and short-term sea level curves (after Haq *et al.*, 1987); the Late Miocene-Quaternary cycles according to Haq *et al.*, (1987) curve recalibrated by Gorini *et al.* (2014). The Plio-Pleistocene cycles according to Miller *et al.* (2005).

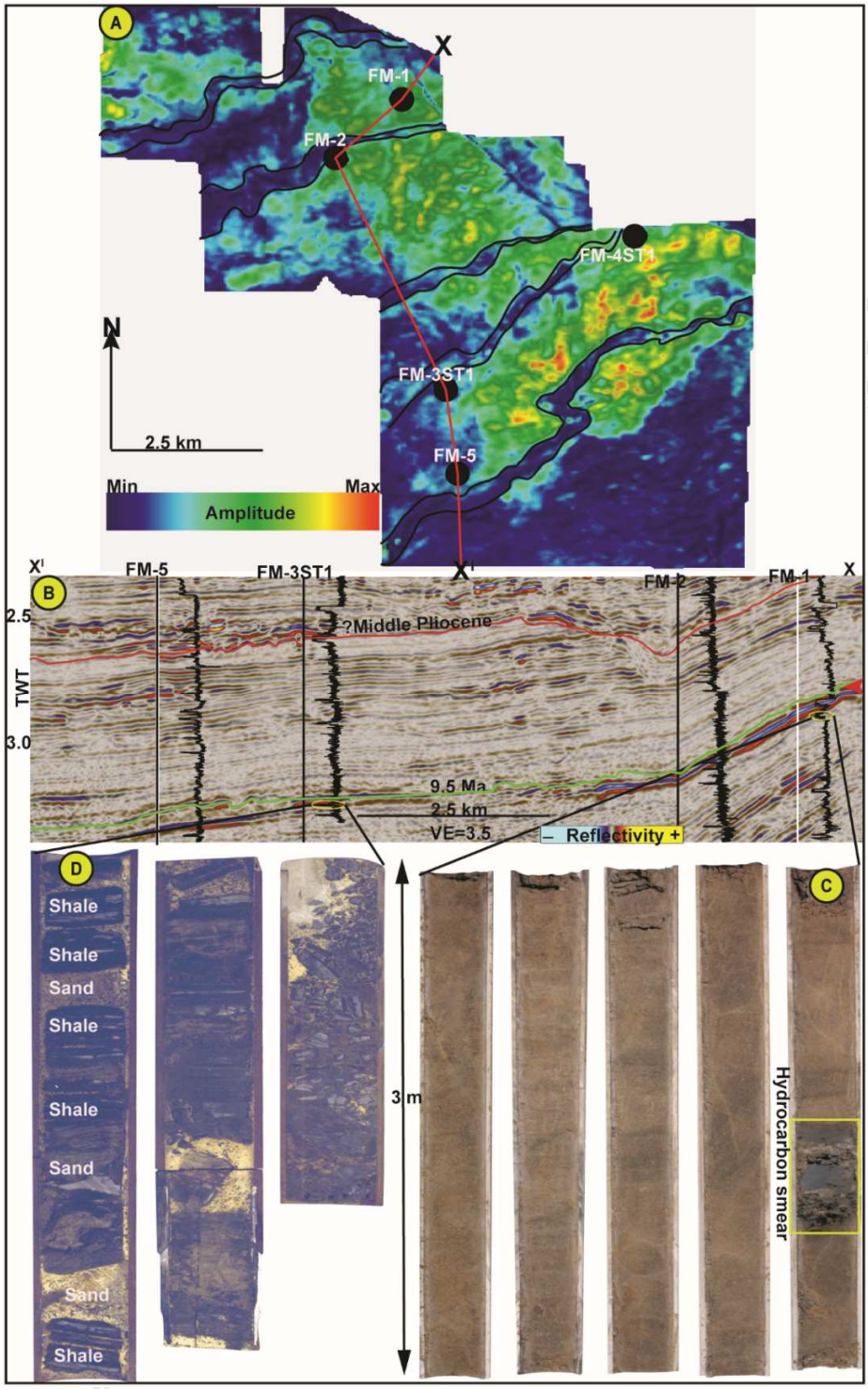


Fig. 9. A: RMS amplitude map at 3.3 seconds (twt) in the C_{bh} facies showing channel architectural patterns. B: Corresponding seismic line illustrating the associated seismic facies. C, D: Core data from the FM-1 and FM-3ST1 wells showing the lithological content.

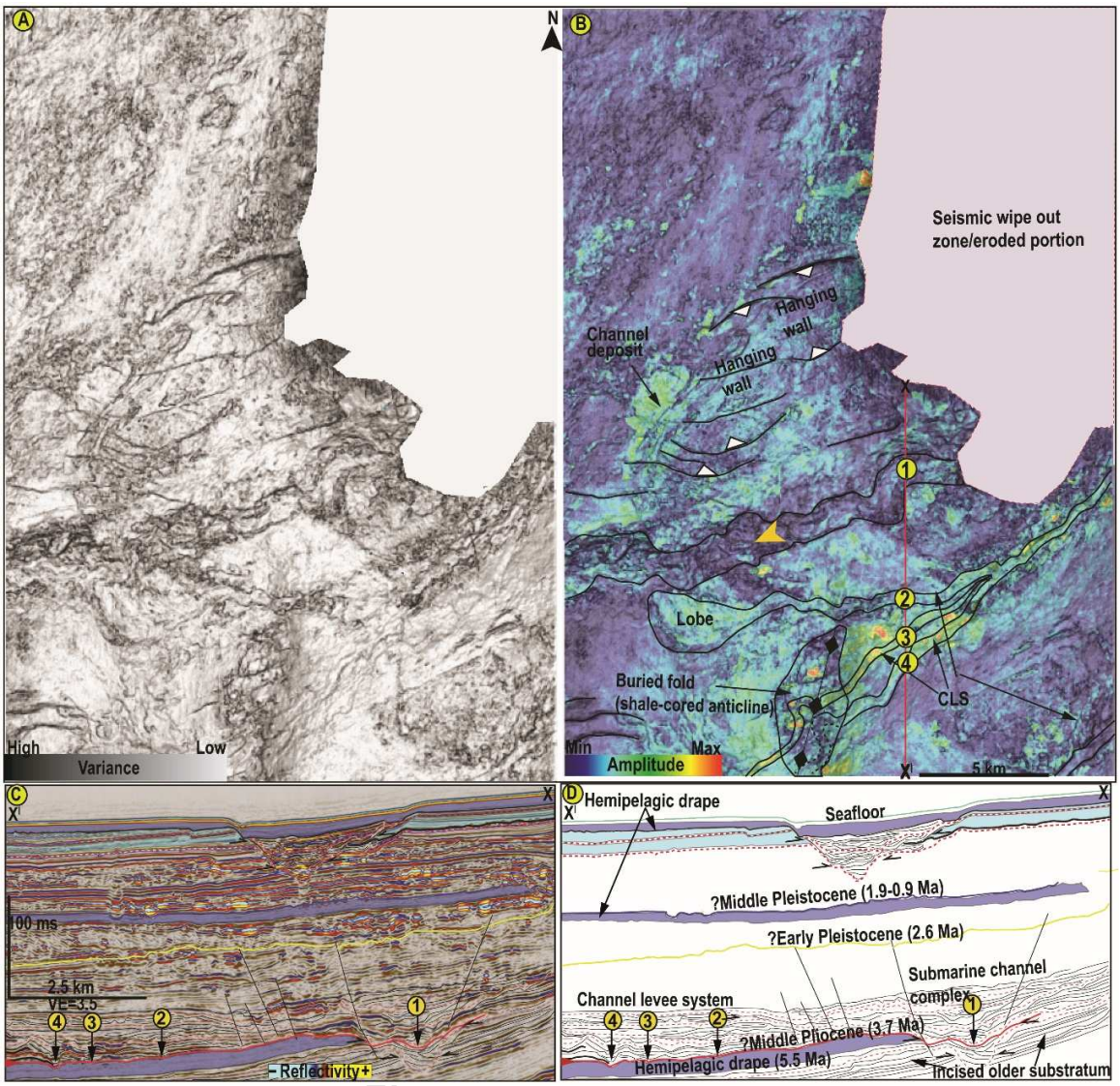


Fig. 10. A: Uninterpreted horizon (variance attribute) slice of the erosional event at the base of Unit 6. B: RMS amplitude extraction on the base of Unit 6 draped on panel A. The main submarine channel complex (labeled 1) and channel levee systems (labelled CLSs 2, 3 and 4) are illustrated. C, D: Interpreted seimic line and line drawing showing the architecture of the channels. Yellow arrow (panel B points to paleo-flow direction), while red arrow (part D) points to the level of amplitude extraction. Note the narrow, low sinuosity, erosional character and E-W orientation of the main submarine channel complex 1. Note also the ability of the CLSs 2 and 3 to cross paleo-relief features associated with the buried shale-cored anticline/fold.

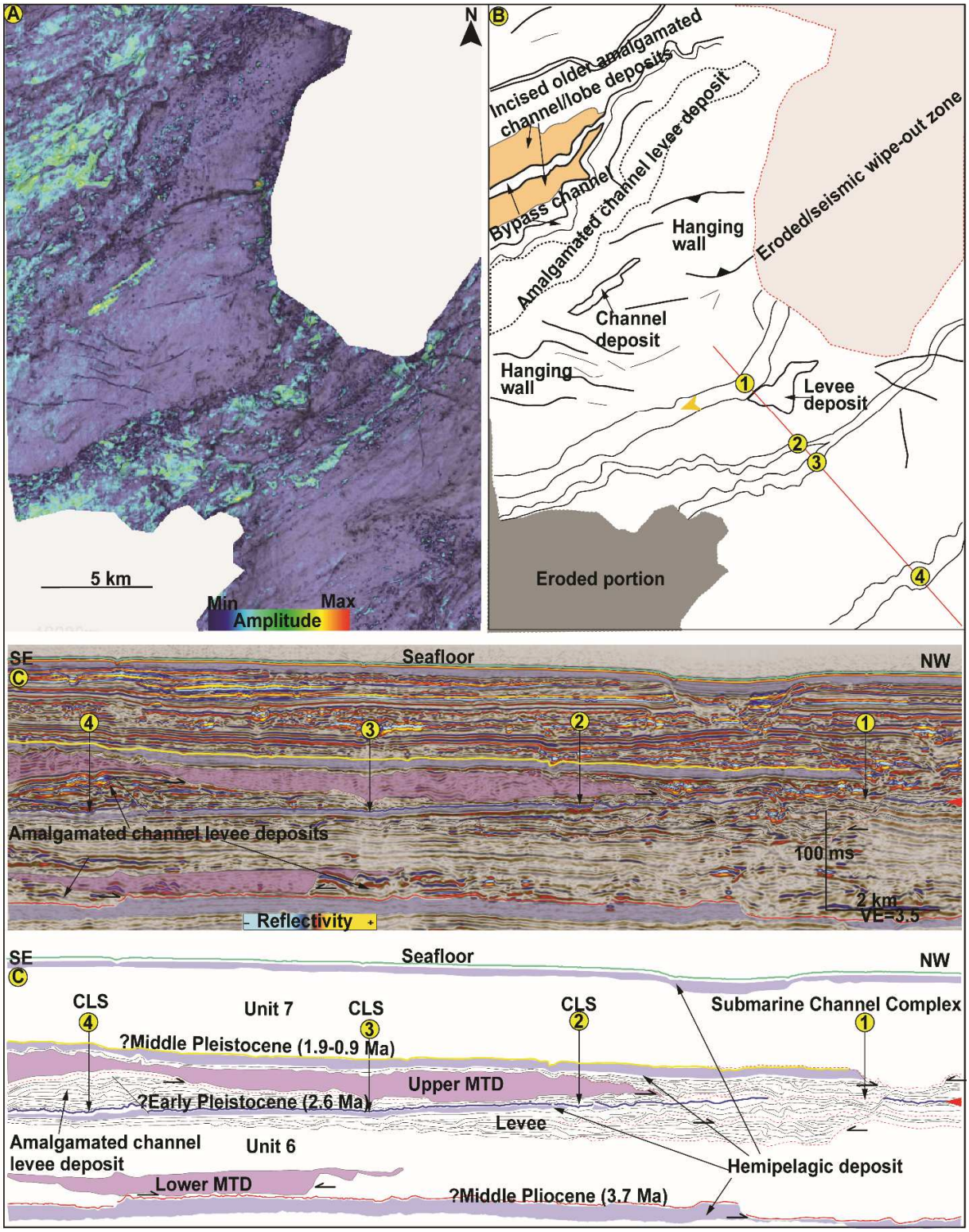


Fig. 11. A: Uninterpreted RMS amplitude map of a channel levee system near the top of Unit 7 draped on the horizon (variance attribute) slice. B: Interpretation of panel A illustrating narrow,

erosional low sinuosity submarine channel complex 1 and moderate sinuosity CLSs (labeled 2, 3 and 4). C: Seismic line and line drawing illustrating the architectures of the channels. Red arrow (panel C) points to the level of amplitude extraction. Note the prsence of bifurcating, bypass CLS that incised older amagamated channel/lobe deposits in the NW corner of the map and the truncation of amalgmated channel levee deposits by the lower and middle MTDs.

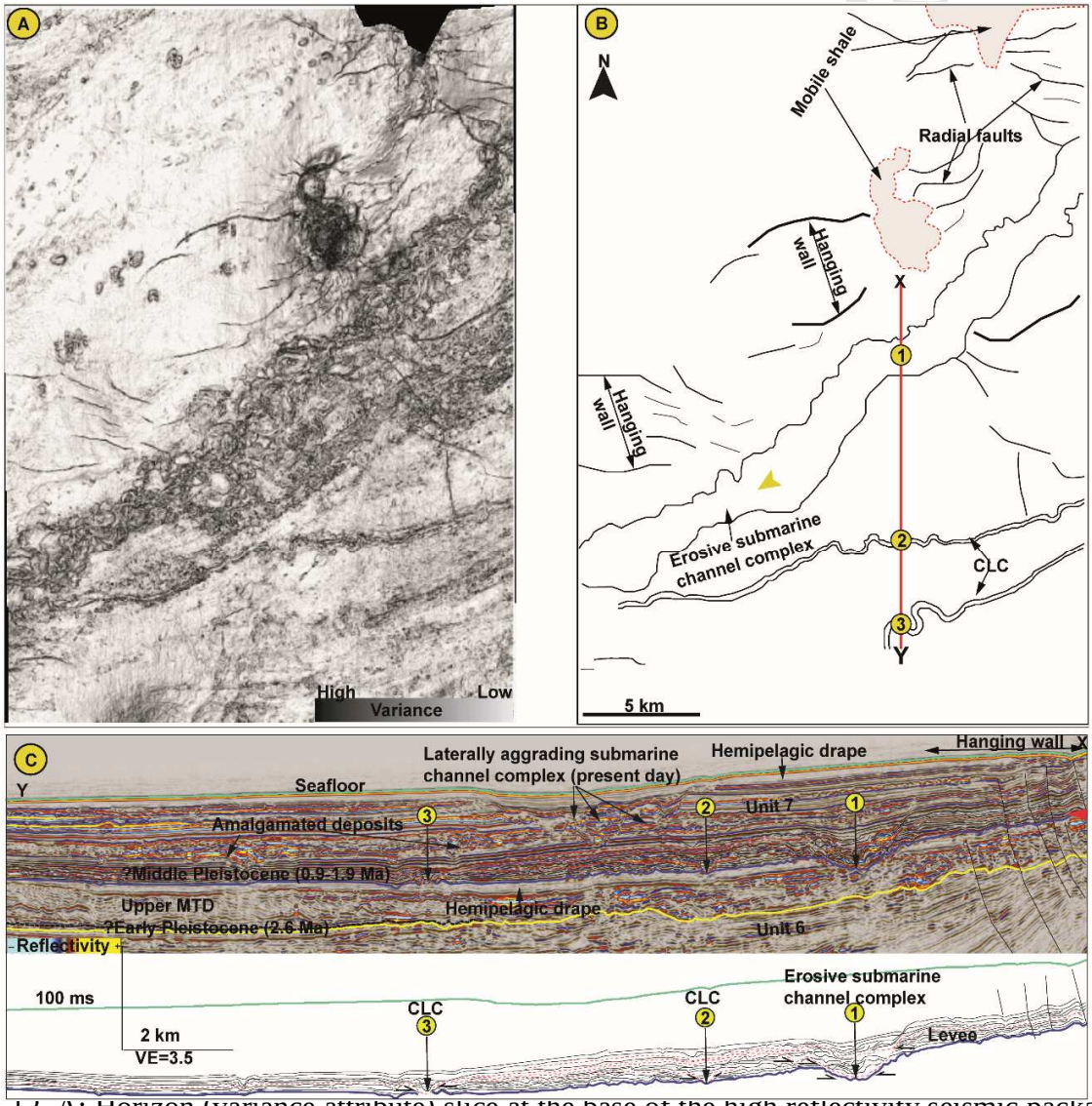


Fig. 12. A: Horizon (variance attribute) slice at the base of the high reflectivity seismic packages above the base of Unit 7 (blue line). Note the presence of wide, highly sinuous submarine

channel complex (labeled 1 in panels B and C), and highly sinuos CLSs (labeled 2 and 3). Note also the erosional character and northward shift of the main submarine channel complex 1 toward the mobile shale zone in the NE and its NE-SW orientation.

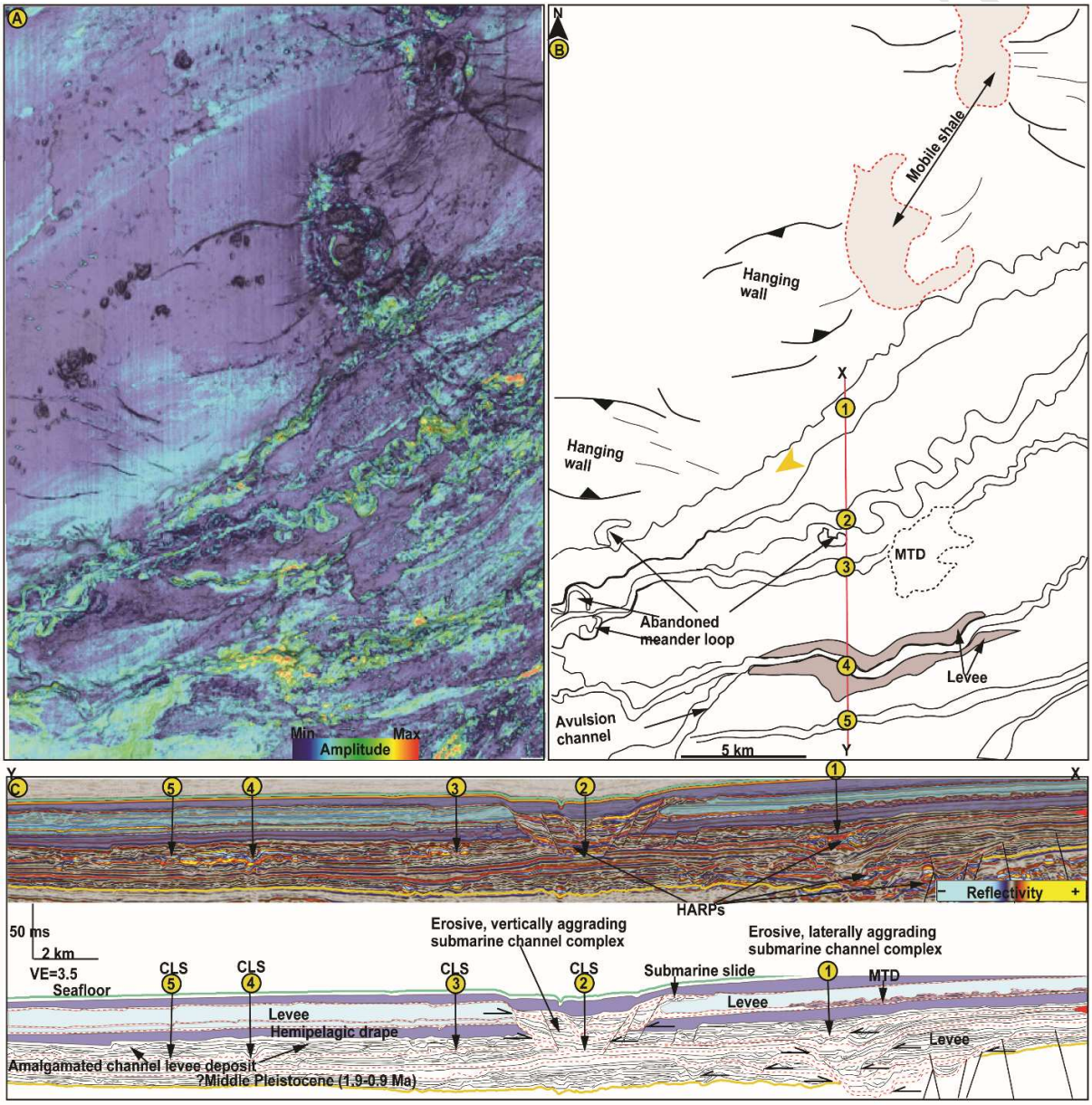


Fig. 13. A: Uninterpreted RMS amplitude map at 1.9 seconds (twt) draped on horizon (variance attribute) slice. B: 3D geomorphological interpretation of panel A showing the architectures of submarine channel complex (labeled 1), CLSs 2 to 5 and faults. C: Seismic line and line drawing

illustrating the complex cut and fill architecture/lateral aggradation of the main submarine channel complexes 1. Note: (I) The erosive nature of the main channel complex compared to the aggrading CLSs 3 to 5. (II) The presence of abandoned meander loops associated with the meandering CLS 2. (III) The presence of an avulsion channel downstream of levee deposit adjacent to CLS 4. (IV) The overall decrease in RMS amplitude downstream along the CLS 4 and the corresponding increase upstream along the avulsion channel.

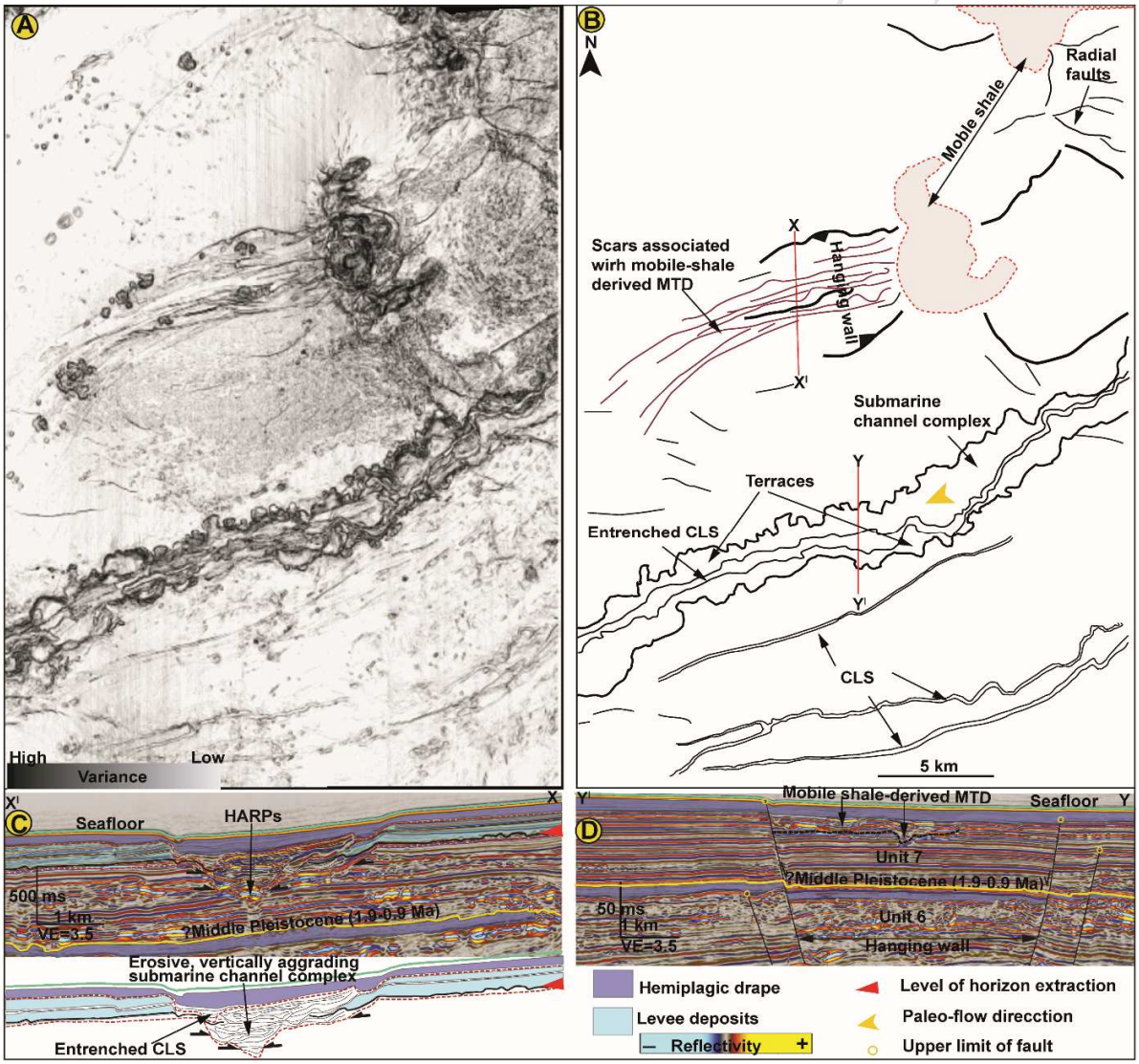


Fig. 14. A, B: Uninterpreted and interpreted horizon (variance attribute) slice at 1.8 seconds (twt) showing the presence of submarine channel complexes (yellow arrow), sinuous CLSs, mobile

shales, radial faults and lineated scars associated with mobile shale-derived MTDs. C: Seismic lines illustrating the erosional character and rough edges of the submarine channel complex. D: Seismic line showing the conformable/slightly deformed, high amplitude seismic packages associated with mobile-derived MTDs. Note the E-W orientation, presence HARPs (panel C), terraces and entrenched CLS in the main submarine complex.

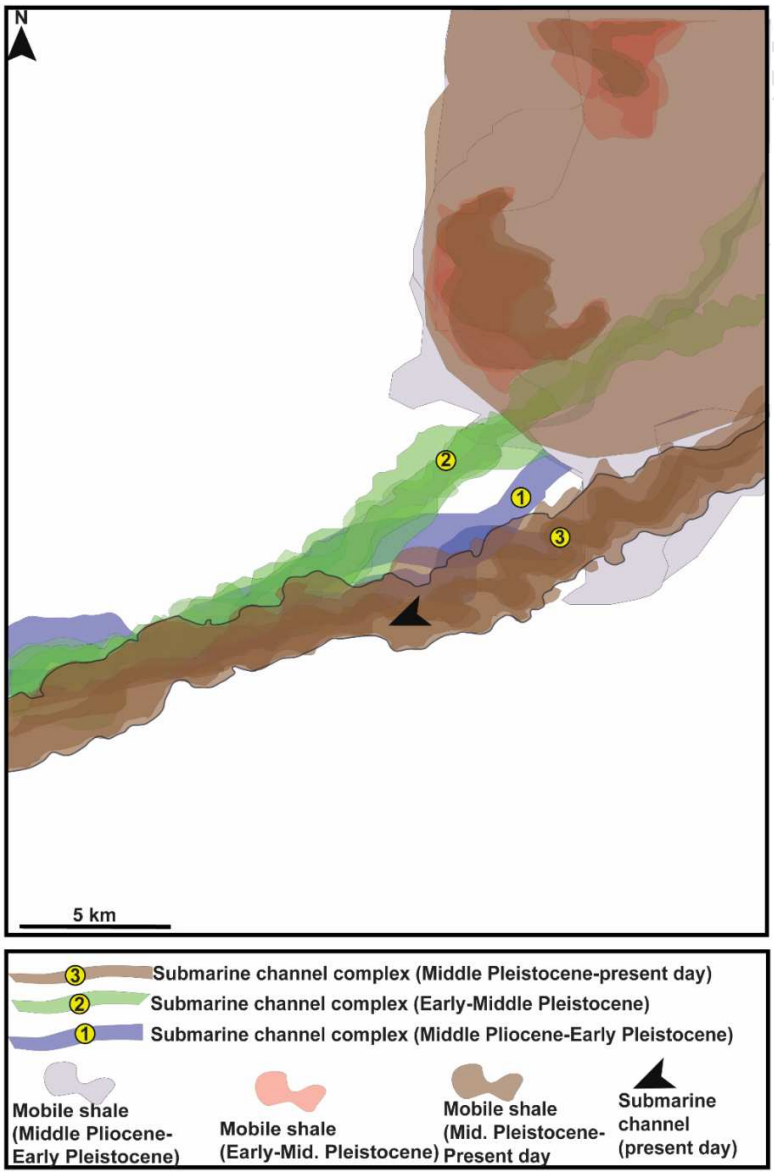


Fig. 15. Shale tectonics and submarine channel complex evolution from Middle Pliocene to present day. Note E-W orientation of the channel complex during the Middle Pliocene-Early

Pleistocene (purple polygon; Unit 6); the NE-SW orientation during the Early-Middle Pleistocene (green polygon; Unit 7) and the E-W orientation from the Middle Pleistocene to present day (brown polygon; Unit 7). Note the confinement of mobile shales in the NE of the study area during the Plio-Pleistocene intervals. See text for more detailed explanation.

ACCEPTED MANUSCRIPT

ACCEPTED MANUSCRIPT

Highlights

- The Neogene stratigraphy of the western Niger Delta slope dates to the Chattian
- Major changes in sedimentary record occurred in the Tortonian and Plio-Pleistocene
- Depositional architecture is controlled by eustasy, sediment supply and shale tectonics
- Depositional sequence in intraslope basins constitutes MTDs, turbidites and hemipelagites
- Channel fills and overbank deposits act as reservoirs while hemipelagites act as seals

ACCEPTED MANUSCRIPT